DEPARTMENT OF MECHANICAL ENGINEERING & MECHANICS
COLLEGE OF ENGINEERING & TECHNOLOGY
OLD DOMINION UNIVERSITY
NORFOLK, VIRGINIA 23529

INVESTIGATION OF ADVANCING FRONT METHOD FOR GENERATING UNSTRUCTURED GRID

By

A. M. Thomas, Graduate Research Assistant

and

S. N. Tiwari, Principal Investigator

Progress Report
For the period ended May 31, 1992

Prepared for
National Aeronautics and Space Administration
Langley Research Center
Hampton, Virginia 23665

Under
Research Grant NCC1-68
Dr. Robert E. Smith Jr., Technical Monitor
ACD-Computer Applications Branch

June 1992

DEPARTMENT OF MECHANICAL ENGINEERING & MECHANICS
COLLEGE OF ENGINEERING & TECHNOLOGY
OLD DOMINION UNIVERSITY
NORFOLK, VIRGINIA 23529

INVESTIGATION OF ADVANCING FRONT METHOD FOR GENERATING UNSTRUCTURED GRID

By

A. M. Thomas, Graduate Research Assistant

and

S. N. Tiwari, Principal Investigator

Progress Report
For the period ended May 31, 1992

Prepared for
National Aeronautics and Space Administration
Langley Research Center
Hampton, Virginia 23665

Under
Research Grant NCC1-68
Dr. Robert E. Smith Jr., Technical Monitor
ACD-Computer Applications Branch

Submitted by the
Old Dominion University Research Foundation
P.O. Box 6369
Norfolk, Virginia 23508-0369

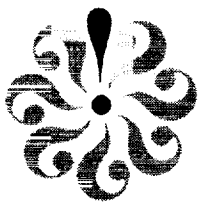

June 1992

FOREWORD

This is a progress report on the research project " Numerical Solutions of Three-Dimensional Navier-Stokes Equations for Closed - Bluff Bodies" for the period ended May 31, 1992. Specific efforts during this period were directed in the area of "Investigation of Advancing Front Method for Generating Unstructured Grid."

This work was supported by the NASA Langley Research Center through Cooperative Agreement NCC1-68. The cooperative agreement was monitored by Dr. Robert E. Smith, Jr., of the Analysis and Computational Division (Computer Applications Branch), NASA Langley Research Center, Mail Stop 125.

SUMMARY

Investigation of Advancing Front Method for Generating Unstructured Grid.

A. M. Thomas* and S. N. Tiwari†

Old Dominion University, Norfolk, Virginia 23529

In this report advancing front technique is used to generate an unstructured grid about simple aerodynamic geometries. Unstructured grids are generated using VGRID2D and VGRID3D software. Specific problem considered are NACA 0012 airfoil, bi-plane consisting of two NACA 0012 airfoil, a four element airfoil in its landing configuration and an ONERA M6 wing. Inviscid time dependent solutions are computed on these geometries using USM3D and the results are compared with standard test results obtained by other investigators. A grid convergence study is conducted for NACA 0012 airfoil and compared with structured grid. Structured grid is generated using GRIDGEN software and inviscid solutions computed using CFL3D flow solver.

The results obtained by unstructured grid for NACA 0012 airfoil showed an asymmetric distribution of flow quantities and a fine distribution of grid was required to remove this asymmetry. On the other hand structured grid predicted a very symmetric distribution but when the total number of points were compared to obtain the same results it was seen that structured grid required more number of grid points.

* Graduate Research Assistant, Department of Mechanical Engineering and Mechanics.
† Eminent Professor, Department of Mechanical Engineering and Mechanics.

Table of Contents

LIST OF TABLES

LIST OF FIGURES

1. INTRODUCTION

A problem of great concern in computational fluid dynamics is the generation of suitable grids. Despite considerable effort devoted toward the development for various grid generation methods, the process of developing a quality grid around a complex configuration and getting a flow solution still remains a challenging task.

A grid is defined as a set of points with appropriate connections between the points. The points act as reference positions within the field at which the flow variables are to be computed and the connections between the points act as pathways for transferring information around the computational domain. In a structured grid the connectivity between the points is explicitly defined through a curvilinear coordinate system. In an unstructured grid the connectivity can be arbitrary and therefore must be specified. Solution methods that utilize a structured grid are generally more efficient than an unstructured grid solution method. However unstructured grids provide a much greater degree of flexibility than is available with a structured grid. In particular, unstructured grids can discretize a highly complex domain easily and are suitable for performing localized grid enrichment in solution adaptive methods.

There are a variety of methods for generating unstructured grids. Among the different techniques are Delauny triangulation methods [1], the modified Octree method [2] and the advancing front technique [3]. In the present study, an advancing front technique is used to generate the unstructured grid for a variety of geometries. This method was selected because it does not require a separate library of modules to distribute grid points throughout the domain in

advance like the Delauny triangulation methods. The main disadvantage of the modified Octree method is that it has the difficulty of correctly defining the boundary segments.

There are a number of software available to generate structured grid. Among the various codes available, GRIDGEN [4] code is used to generate structured grid around NACA 0012 airfoil. This code provides an efficient means of developing multiple block grid for complex configurations.

Steady state Euler solutions are computed using USM3D [5] on unstructured grids and CFL3D [6] on structured grids. The results obtained for NACA 0012 airfoil are plotted and compared.

The objective of this report is to describe our experience with the advancing front algorithm for several test problems and to conduct a comparative study with structured grids. Steady state Euler solutions computed on these grids using the USM3D and CFL3D flow solver are presented. The grid generation technique is described in Sec. 2 and the flow solution methods are explained in Sec. 3. The numerical results are presented and discussed in Sec. 4.

2. GRID GENERATION

2.1 Unstructured Grid Generation

In this study unstructured grids are generated around simple 2-D and 3-D geometries. A 2-D version of the unstructured grid generation package (VGRID2D) is used to generate the 2-D grids. The input file contains the points defining the surface of the airfoil with connectivity table. A background grid is then setup which in 2-D is in the form of triangles. The background grid defines the local grid characteristic such as grid spacing. A typical background grid for a NACA 0012 airfoil is shown in Fig. 2.1. The 2-D grid is generated by first placing points on the boundary segments that define the solution domain, and then discretizing the interior region. A program has been developed (GEN3D) that uses the generated 2-D grid and duplicates it in the third direction, to form prism elements. Using the prism centroid, each prism is divided into eight tetrahedral cells.

2.2 Structured Grid Generation.

Structured grid is generated around NACA 0012 airfoil using GRIDGEN software. This software essentially consists of three main codes, GRIDBLOCK, GRIDGEN2D, and GRIDGEN3D. These are discussed below.

GRIDBLOCK : This is used to develop blocking structures and set interblock connections. The surface definition for NACA 0012 airfoil is read in, which is the same as the one used for

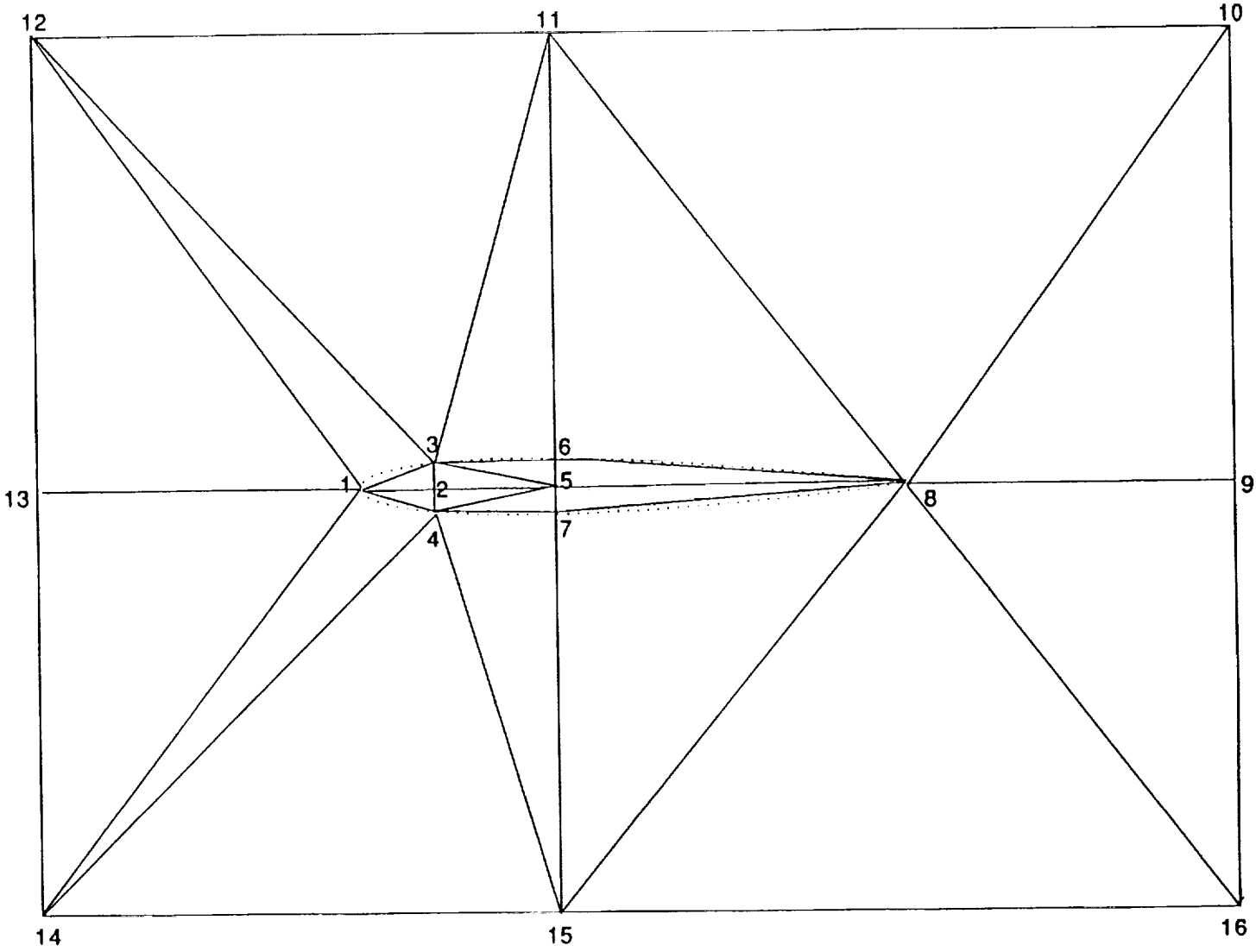

Fig. 2.1 Background grid for NACA 0012 airfoil

the unstructured grid. A single block is used to define the whole domain. The 3-D lines are drawn which define the edges of the block. Computational directions and dimensions are added to the system. After the blocking strategy, flow boundary conditions are applied on all the faces of the block.

GRIDGEN2D : This is used to generate surface grids on the six faces of the block. The grid is generated in components using the block edges. The block edges are then used as boundary condition for block faces and the resulting block faces are used as boundary condition for the block interior. Each of the four edges of a subface is generated before proceeding to the interior. The grid point spacing is defined when distributing points on these edges. The spacing around the airfoil is maintained approximately the same as that in the unstructured grid. Grid points interior to the subface are generated using the elliptic solver to achieve orthogonality near the surface of the airfoil.

GRIDGEN3D : This program is used to distribute points within the interior of the block to generate volume grid. This is accomplished with the batch procedure of GRIDGEN3D and run on the Cray-super computer.

3. GOVERNING EQUATIONS AND METHOD OF SOLUTION

3.1 Structured and Unstructured Grids

The governing equations are the 3-D unsteady Euler equations for inviscid compressible flow. For a bounded domain Ω with a boundary $\partial\Omega$, the time dependent Euler equations in integral form can be written as

$$\frac{\partial}{\partial t}\int\int\int_{\Omega} \bar{Q}\, dv \;+\; \int\int_{\partial\Omega} \bar{F}(\bar{Q}) \bullet \hat{n} dS \;=\; 0 \tag{3.1}$$

$$\bar{Q} = \begin{Bmatrix} \rho \\ \rho u \\ \rho v \\ \rho w \\ \rho e_0 \end{Bmatrix} \quad \text{and} \quad \bar{\mathrm{F}}(\bar{\mathrm{Q}}) = \begin{Bmatrix} (\rho u, \rho v, \rho w) \\ (\rho u^2 + P, \rho uv, \rho uw) \\ (\rho vu, \rho v^2 + P, \rho vw) \\ (\rho wu, \rho wv, \rho w^2 + P) \\ ((\rho e_o + P)u, (\rho e_o + P)v, (\rho e_o + P)w) \end{Bmatrix}$$

In the preceeding equations, ρ is the density, u, v and w are the x, y, z components of the velocity, e_o is the total energy per unit volume and P is the pressure. The equations are non-dimensionalized by a reference density ρ_∞ and speed of sound a_∞. Assuming an ideal gas, the pressure is written as

$$P = (\gamma - 1)\left(e_0 - \frac{1}{2}\rho(u^2 + v^2 + w^2)\right) \tag{3.2}$$

where γ represents the ratio of specific heats.

The inviscid flow field is computed with a three-dimensional upwind flow solver (USM3D) developed at NASA/LaRC [4].The spatial discretization is accomplished with a cell centered finite volume formulation using the flux difference splitting procedure. The solution is advanced in time using a 3-stage Runge-Kutta time stepping scheme. Local time stepping and implicit residual smoothing are used to accelerate the convergence of the solution to a steady state.

For the structured grid the time dependent Euler equations are similar to Eq. (3.1). The unsteady three dimensional equations are solved by a 3-factor implicit time advancement algorithm (CFL3D) which uses a block tridiagonal inversion. Here also local time stepping and implicit residual smoothing are used to accelerate the convergence of the solution to a steady state.

Boundary Conditions

For the solid boundaries the flow tangency condition is imposed. A condition of zero mass and energy flux through the surface is ensured. Characteristic boundary conditions are applied to the far field subsonic boundary. At an outflow boundary, the two tangential velocity components and the entropy are extrapolated from the interior while at an inflow they are specified as having far-field values.

4. RESULTS AND DISCUSSION

Results obtained for different cases and conditions are presented in this section.

Case 1

A NACA 0012 airfoil has been used to validate the algorithm developed. The program considers the 2-D grid points and extends them to a 3-D configuration compatible to the flow solver. The computational domain is bounded by a rectangular box with boundaries at $-10 \leq x \leq 10$, $0 \leq y \leq 2.0$, $-10 \leq z \leq 10$, where the airfoil chord length is one. Initially a coarse grid was generated from VGRID2D consisting of 112 cells, 585 points with 53 boundary points (Fig. 4.0). After going through the 3-D algorithm in which five planes were specified, the 3-D configuration had 35584 cells, 7373 points with 1344 boundary points.

The computations were performed at a CFL number of 4.0 and Mach number of 0.5 with zero angle of attack. For this case, the flow field should be symmetrical about the airfoil and no shock should occur. The solutions were started from free stream initial conditions with the first order scheme. When the RMS average of all residuals dropped by one order of magnitude the solver was switched on to the higher order scheme.

Figure 4.1 shows the convergence history with a decrease of approximately 2.5 orders of magnitude. This figure also shows the total lift and drag which are seen to be constant throughout the computational period.

The percentage of total pressure loss over the surface is shown in Fig. 4.2. It can be seen that the pressure losses are symmetrical about the airfoil. The maximum magnitude of the pressure loss was observed to be 0.04 %. Theoretically, there should be no loss of total pressure

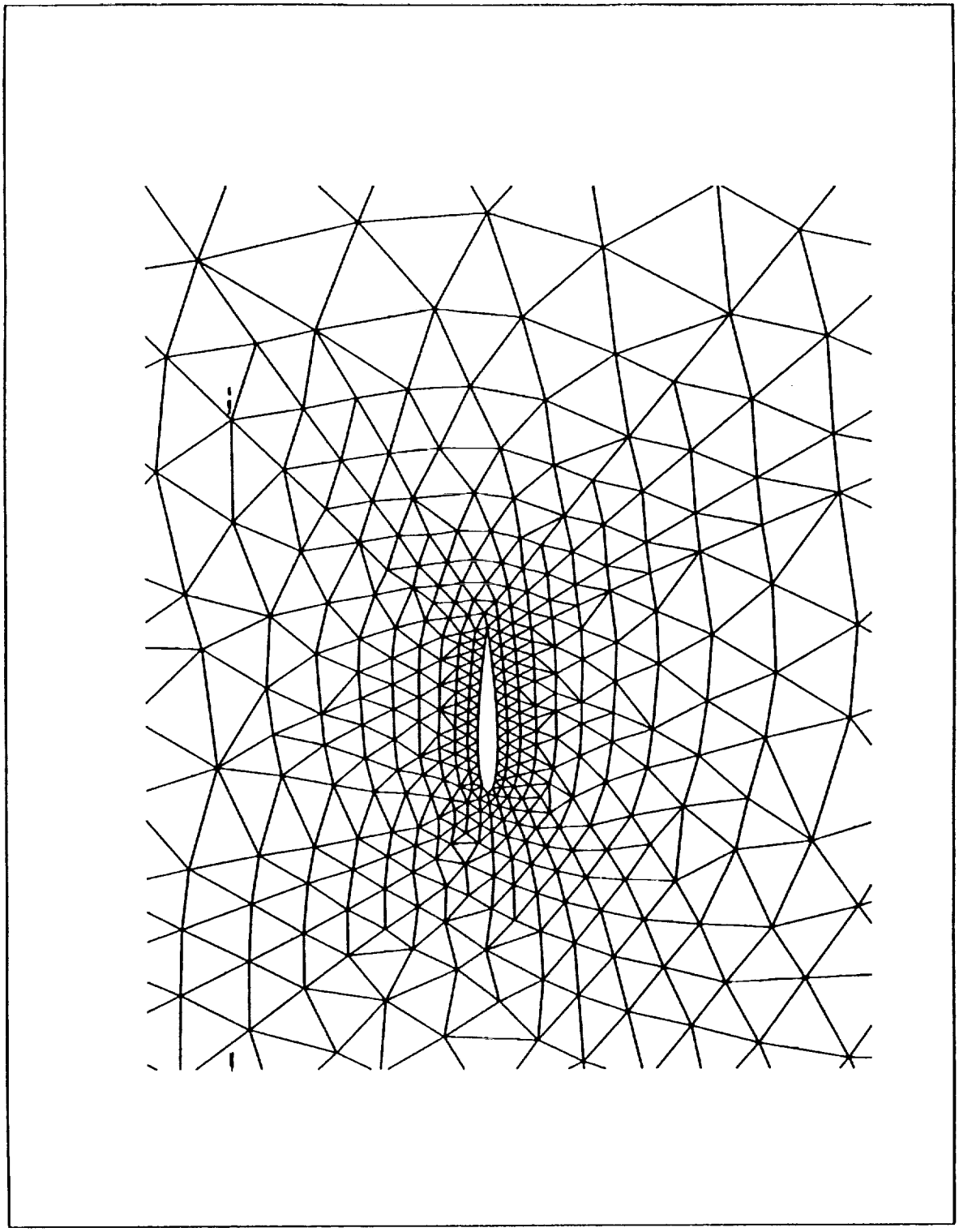

Fig. 4.0 Initial coarse mesh for NACA 0012 airfoil.

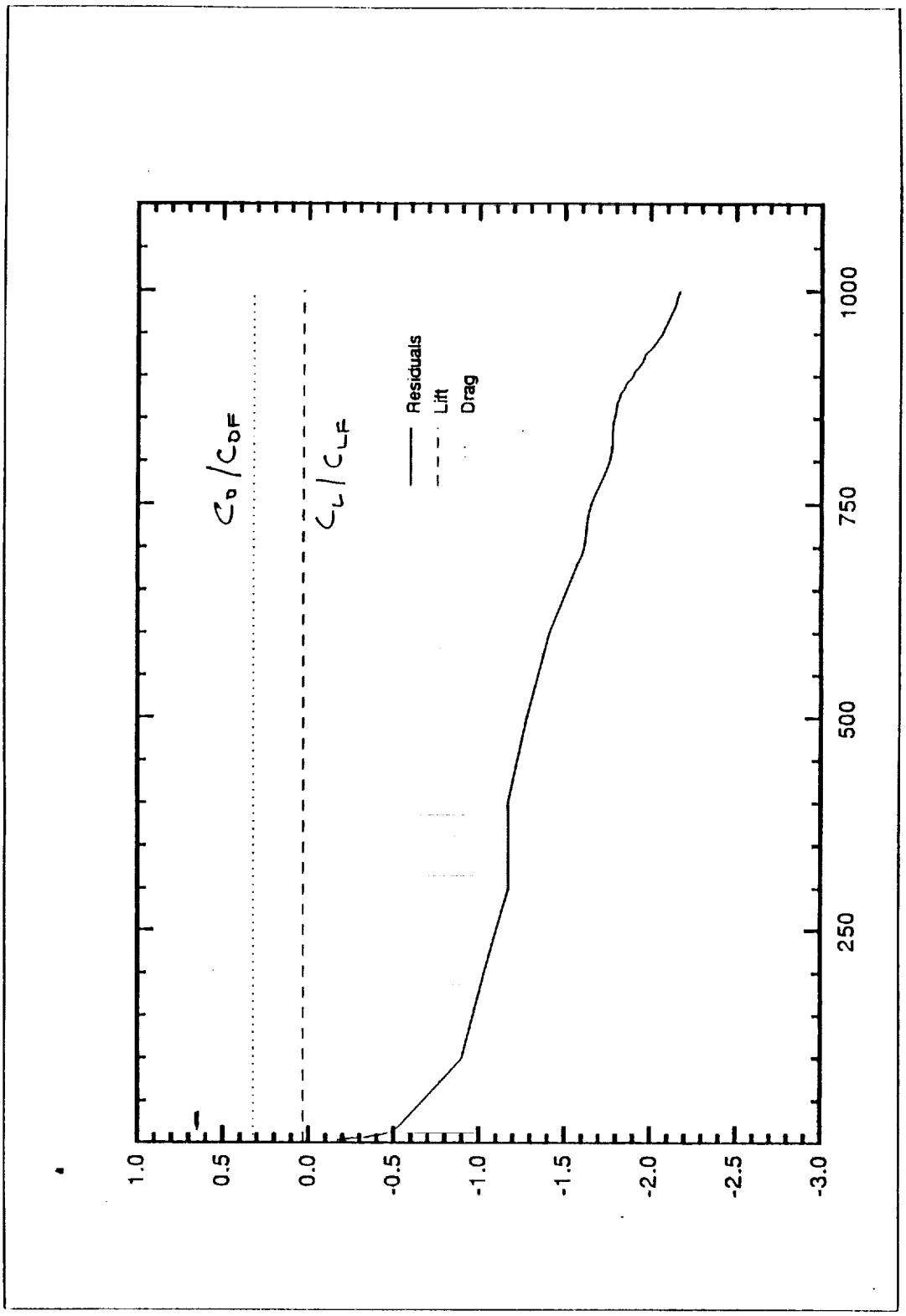

Fig. 4.1 Convergence history for the coarse grid.

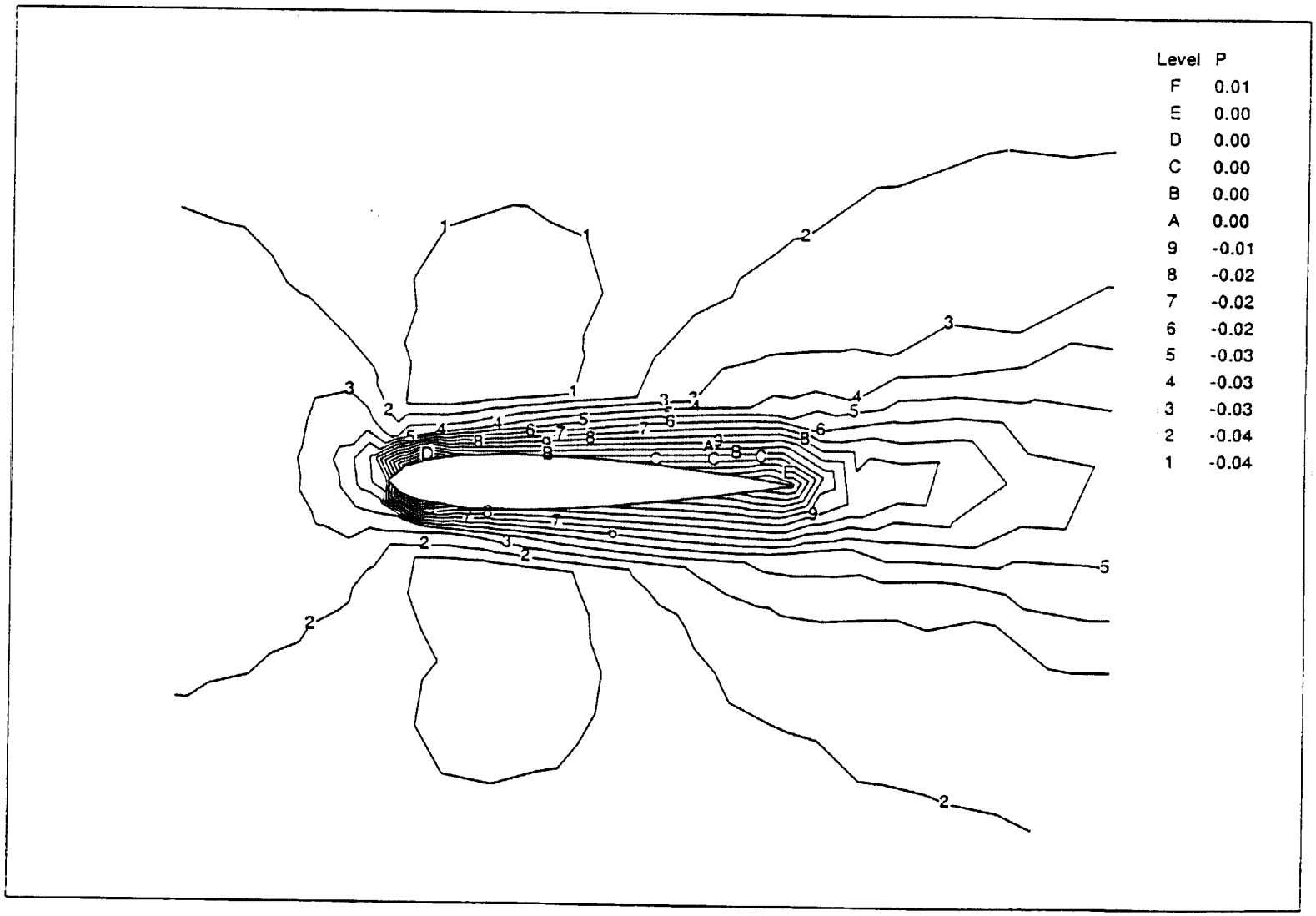

Fig. 4.2 Percentage of total pressure loss over the upper and lower surface.

for this test case because the flow is an isentropic process. The observed pressure losses are due to numerics alone.

Figures 4.3 show the Mach number contours. It can be seen from the figure that the computed flow field is symmetric and free of shocks.

Figure 4.4 shows the coefficient of pressure on the upper and lower surfaces. Since there was no shock, the two curves are approximately symmetrical and no abrupt changes are observed. Theoretically the two curves should lie on top of each other because of the symmetric flow conditions. The deviation in the curve may be due to the coarseness of the grid.

To investigate the asymmetric Cp distribution, a parametric study is conducted and compared with the results from the structured grid. A medium fine grid is selected which has 76 points on the airfoil and a total of 1583 points with 3054 cells. Figure 4.5 shows the plot of the grid in 2-D. The initial condition for this test case is obtained by linearly interpolating the converged coarse grid solution onto the new grid. Figure 4.6 shows the convergence history for this case. The solution was started with a second order differencing scheme but after 150 iterations the solution appeared to be diverging. At this point the solver was switched back to the first order scheme and the solution converged with approximately three orders of magnitude reduction in the residuals. Figure 4.7 shows the Mach number contour plot. Figure 4.8 shows the Cp variation over the upper and lower surfaces. In the Cp plot there is now much better agreement between the upper and lower surface results.

Next a very fine grid is selected in which 163 points are located on the airfoil and the 2-D grid contains a total of 2582 points and 4961 cells. Figure 4.9 shows the grid distribution. The converged solution from the medium fine grid is interpolated on to the fine grid to provide a better initial condition for this test case. In accordance with the approach used in the previous

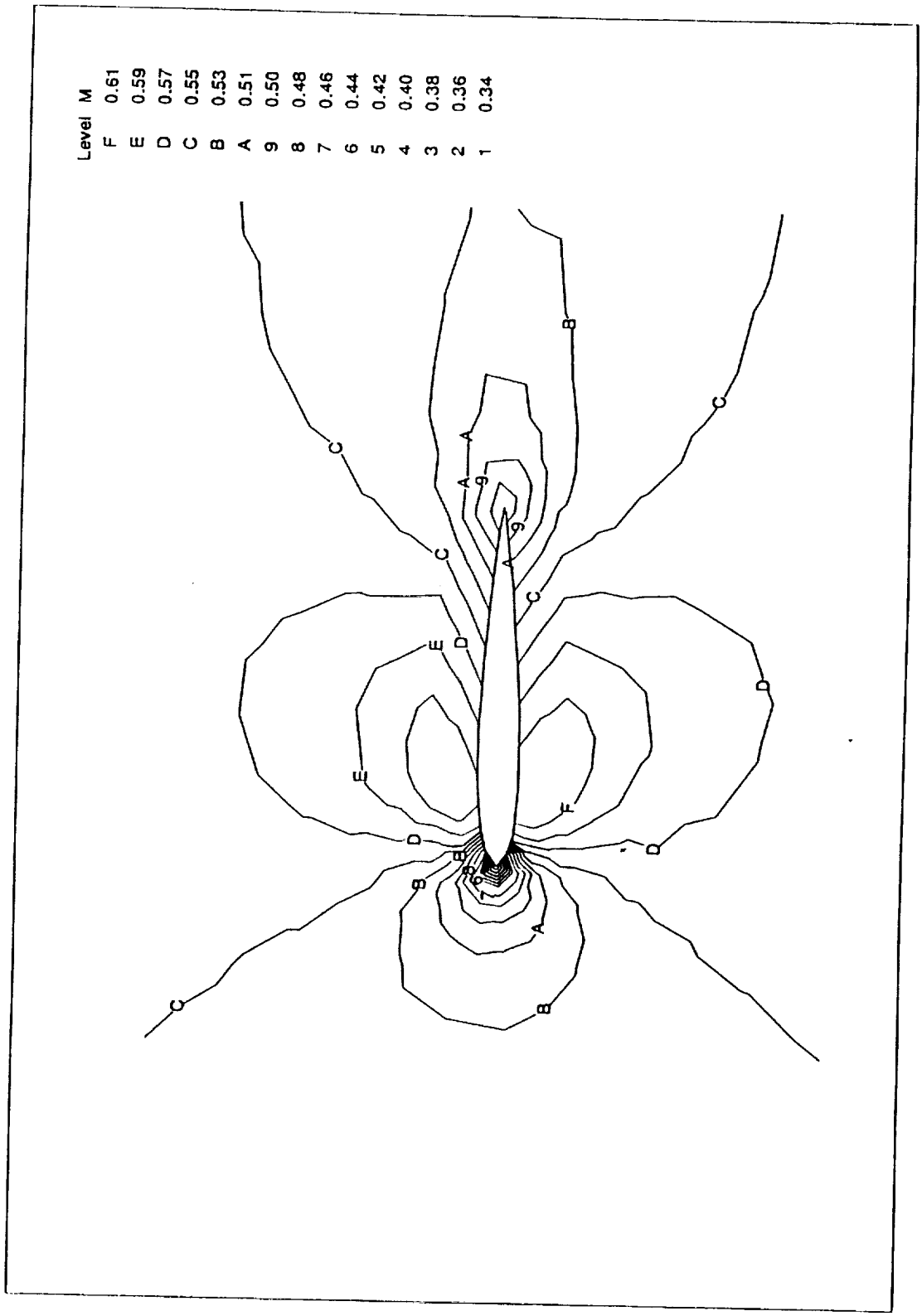

Fig. 4.3 Mach number contours for NACA 0012 airfoil ($M_\infty = 0.5$, $\alpha = 0$).

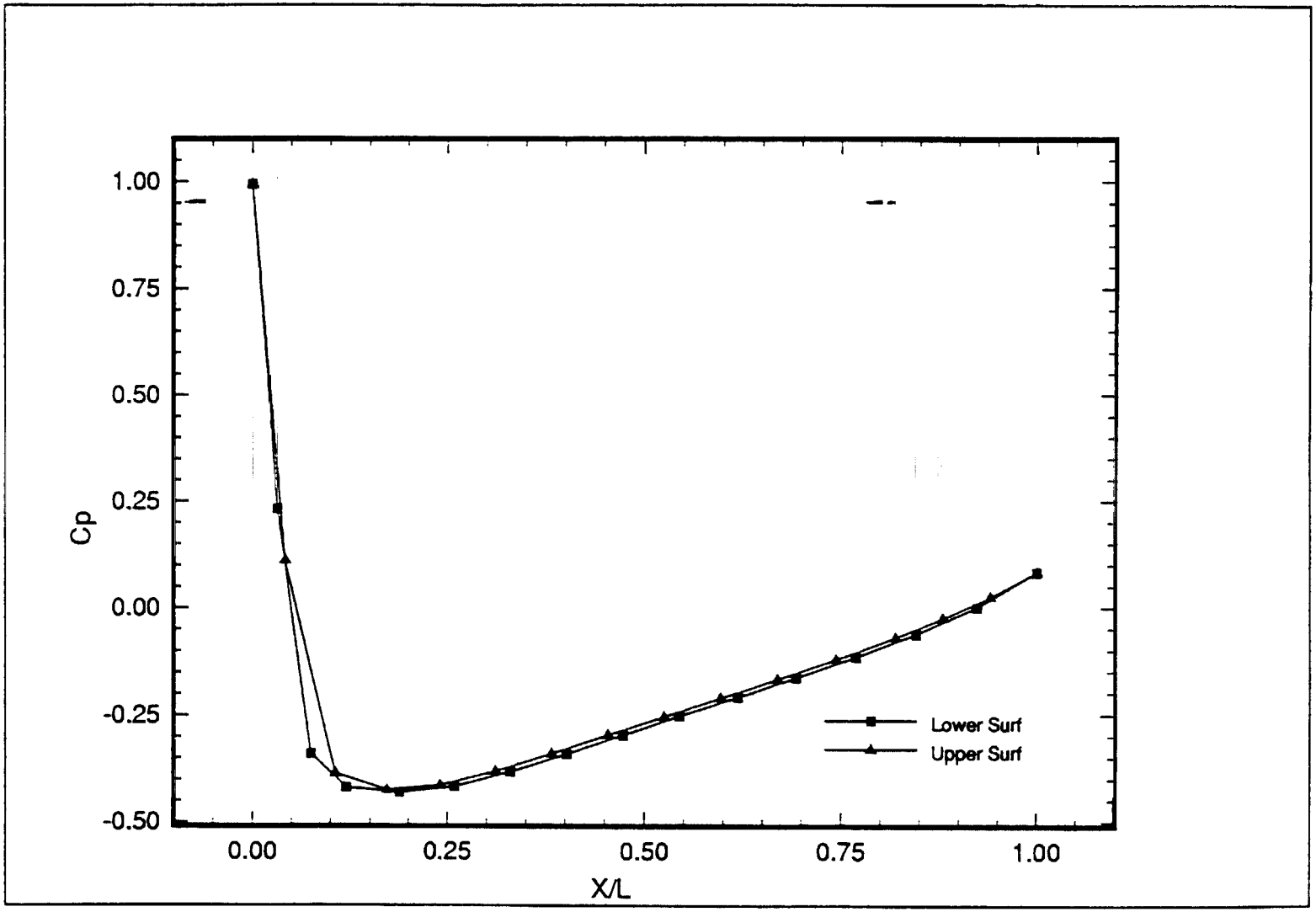

Fig. 4.4 Variation of coefficient of pressure for the upper and lower surface.

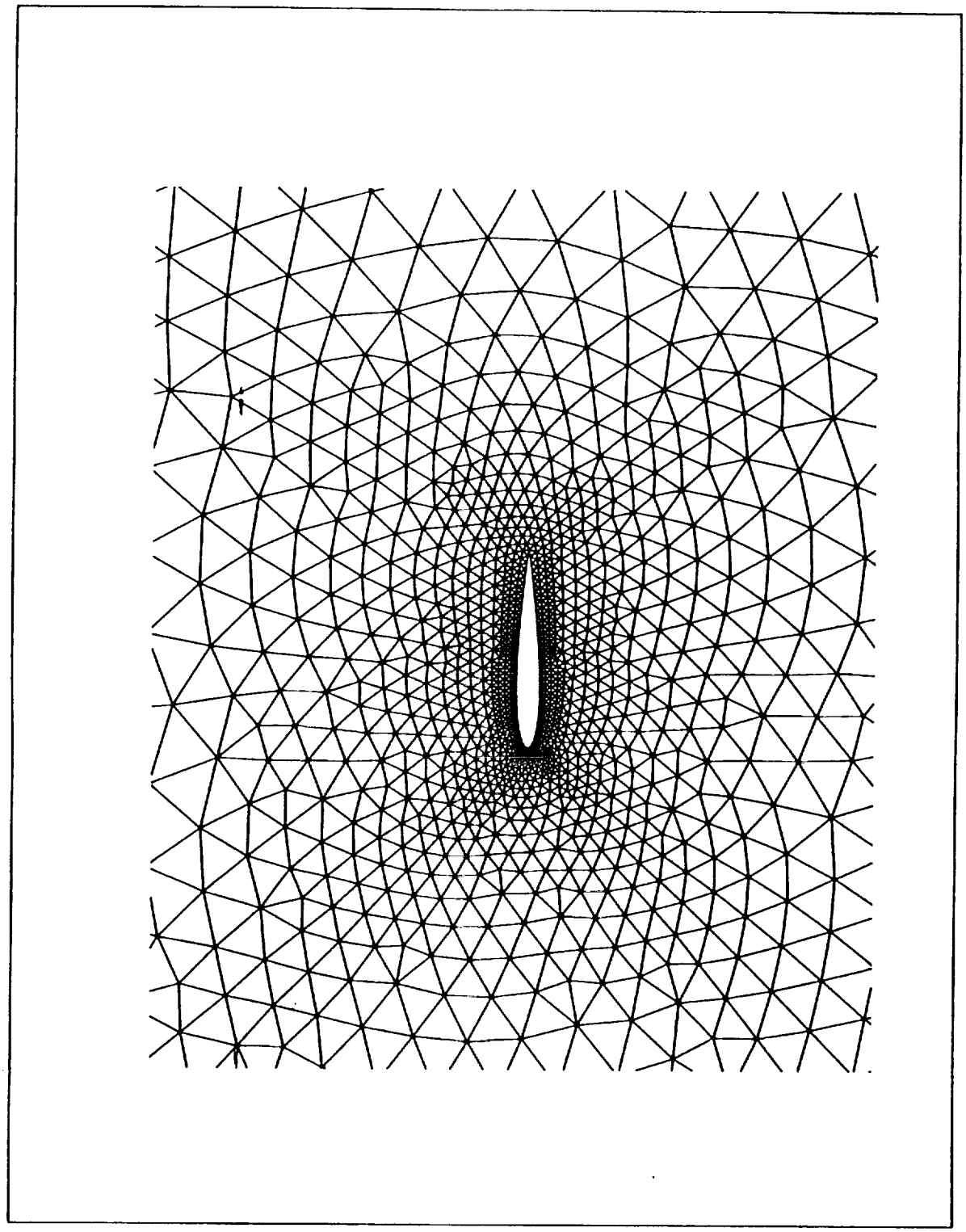

Fig. 4.5 Medium fine mesh for NACA 0012 airfoil.

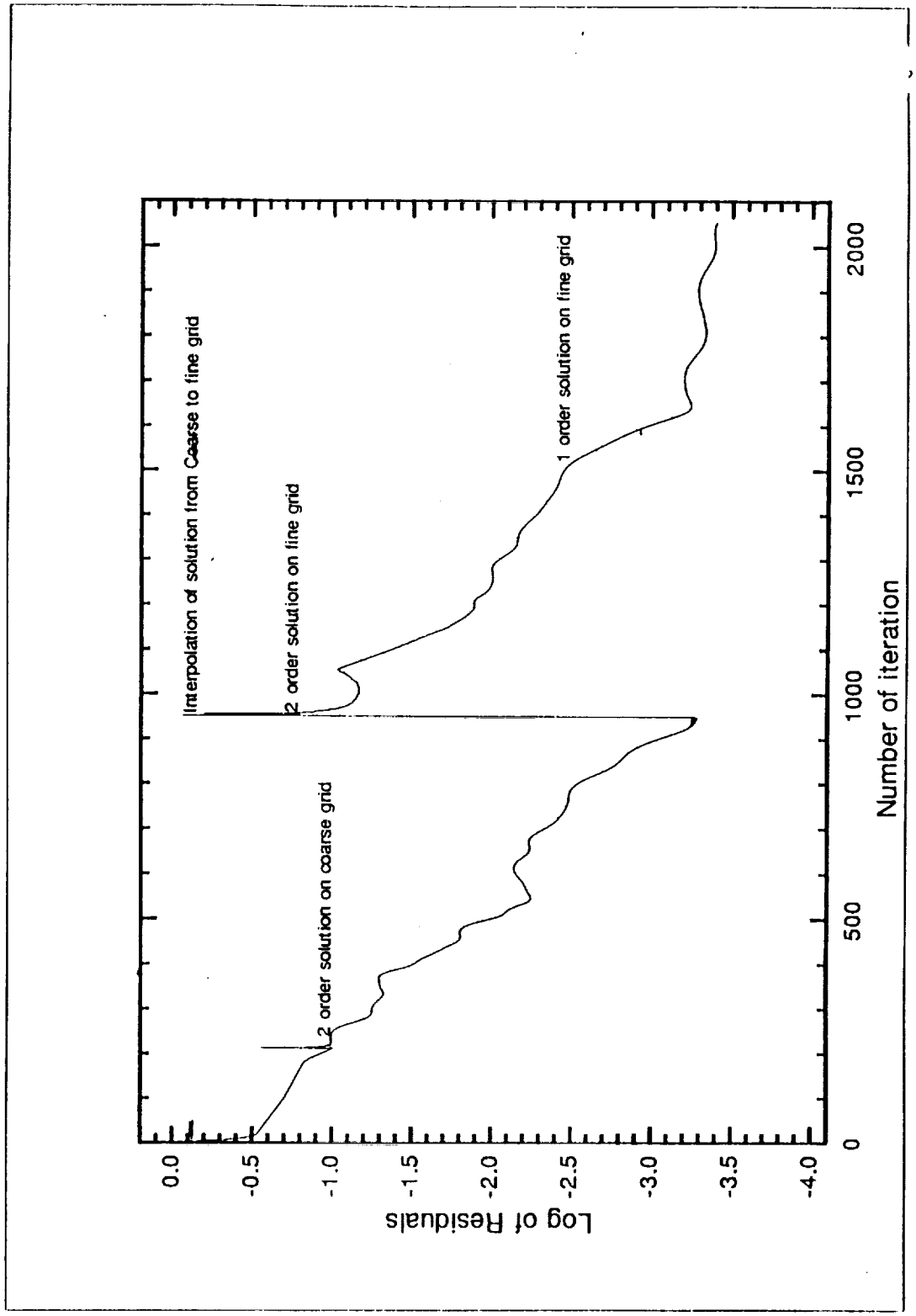

Fig. 4.6 Convergence history on medium fine grid with initial condition interpolated from coarse grid.

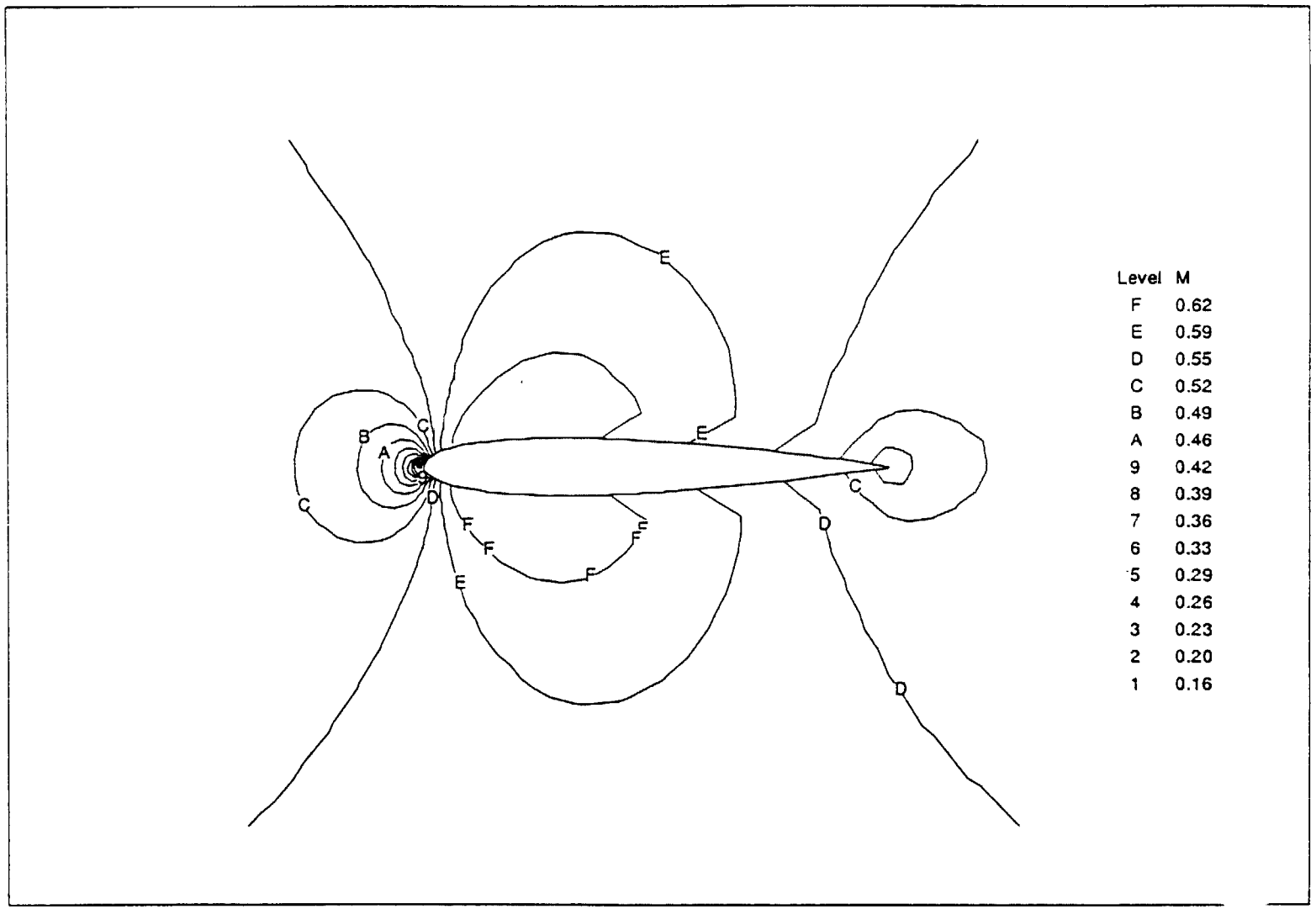

Fig. 4.7 Mach number contours for NACA 0012 airfoil ($M_\infty = 0.5$, $\alpha = 0$).

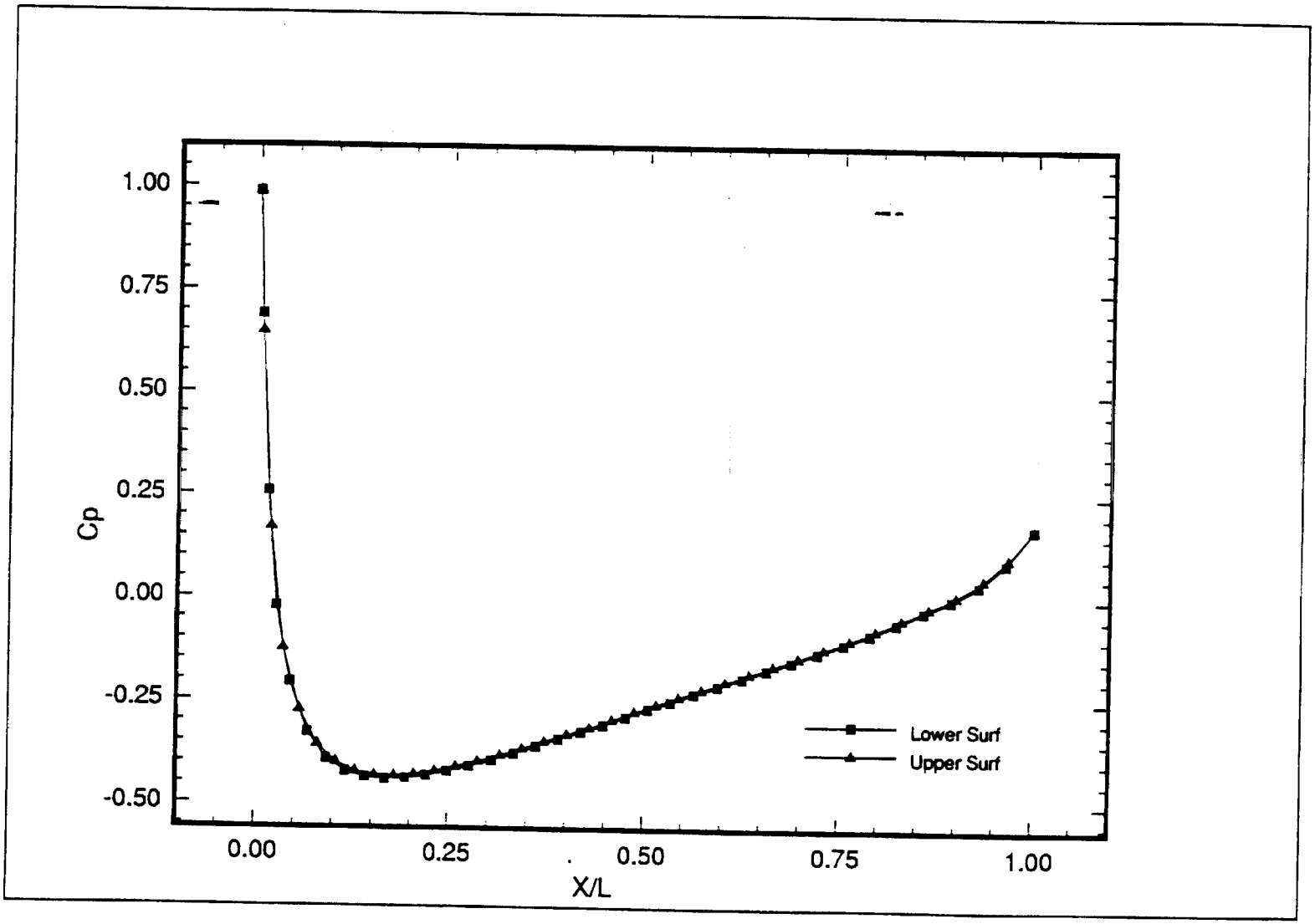

Fig. 4.8 Variation of coefficient of pressure for the upper and lower surface.

test case, the solution was obtained with a first order scheme. Figure 4.10 shows the convergence history for the entire parametric study. Figure 4.11 shows the Cp distribution. For this test, the curves in the Cp plot have very good agreement. The Mach number contour plot is similar to the medium fine grid test case and hence not shown here.

To obtain a good resolution of the contour plots, the grids were concentrated near the nose and tail of the airfoil. The 2-D grid contained 120 points on the airfoil and a total of 2193 points and 4229 cells. Figure 4.12 shows the grid distribution. The convergence history is illustrated in Fig. 4.13. The solution was started from a free stream initial condition with a first order scheme, and when the residuals dropped by one order of magnitude the solver automatically switched over to a second order scheme. A steady state solution was obtained with approximately two orders of magnitude reduction in the residuals. Figure 4.14 shows the Mach number plot where a clear resolution is seen near the nose and tail of the airfoil. Figure 4.15 shows the Cp distribution. Comparison of pressure distribution for the four different cases is shown in Figs. 4.16 and 4.17. The results show that the solution improves with the increase in the number of grid points on the airfoil. Hence it is concluded that a very close resolution of the grid point is required near the airfoil to attain a satisfactory result.

CASE 2

To confirm the results obtained from the unstructured grid, and to have a comparative study, structured grid was generated around the same airfoil with GRIDGEN code.

The physical dimensions were maintained the same as that in the unstructured grid. A C-H type grid was generated and computations were performed with a Mach number of 0.5 at zero angle of attack.

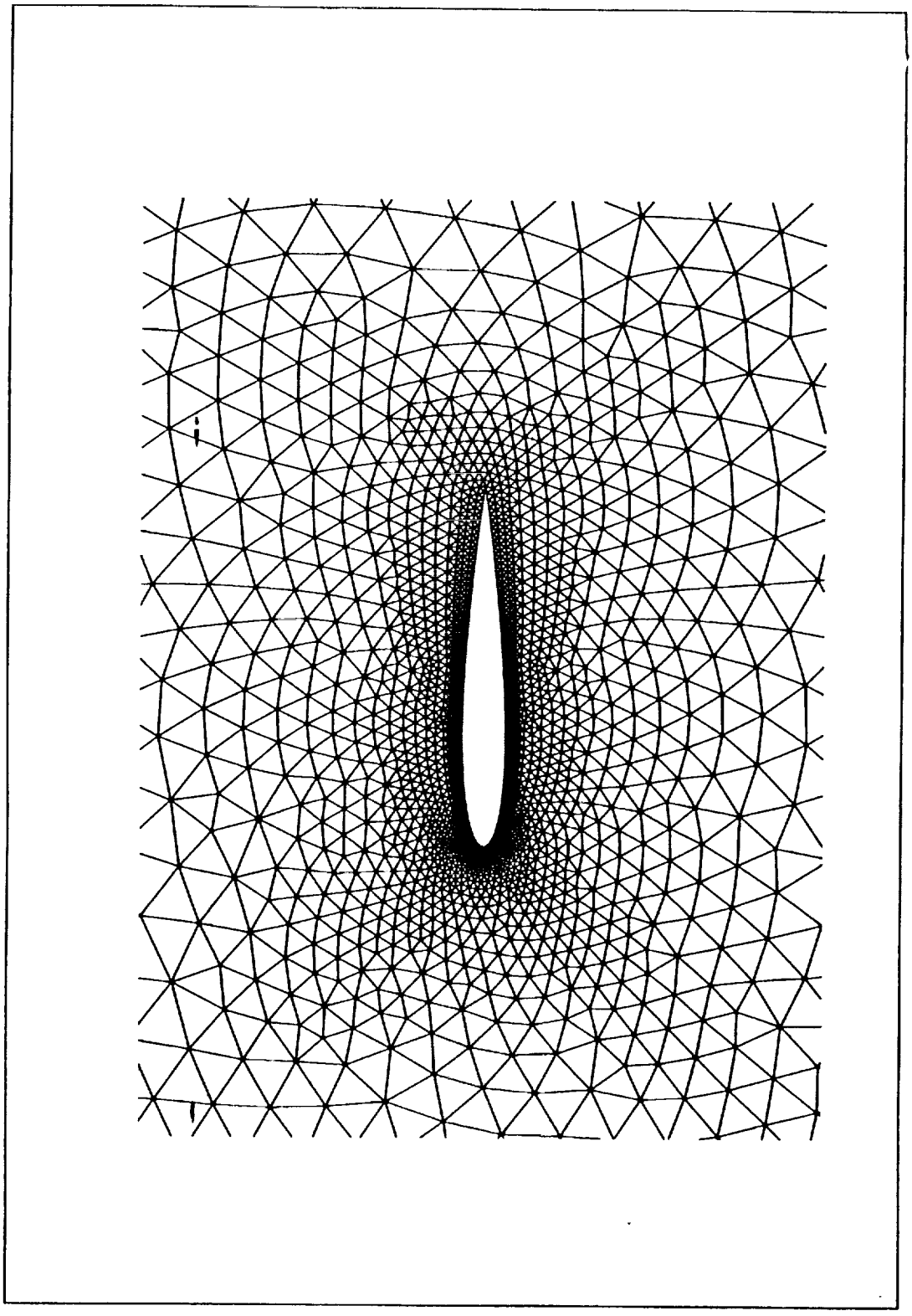

Fig. 4.9 Fine mesh for NACA 0012 airfoil.

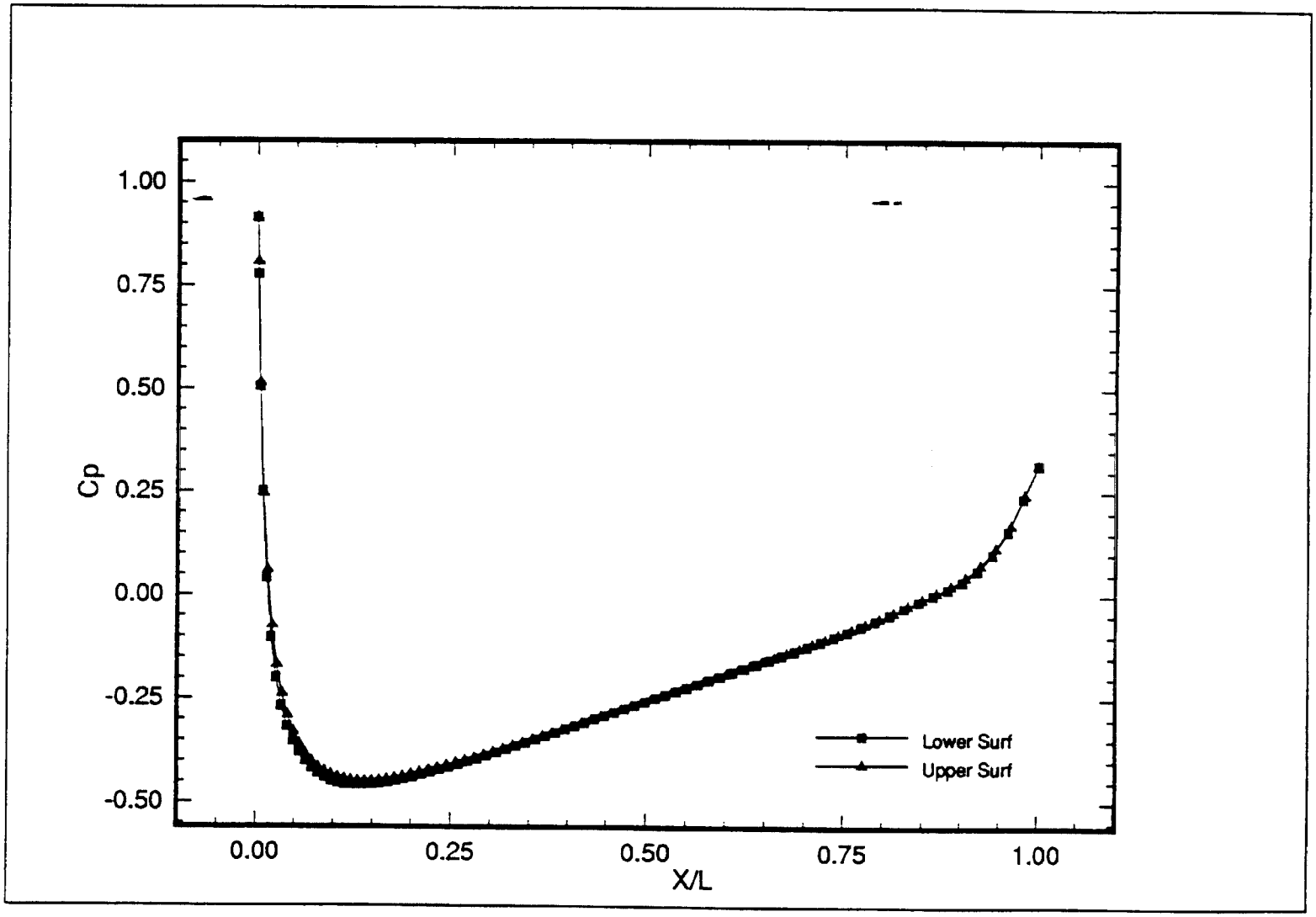

Fig. 4.11 Variation of coefficient of pressure over the upper and lower surface.

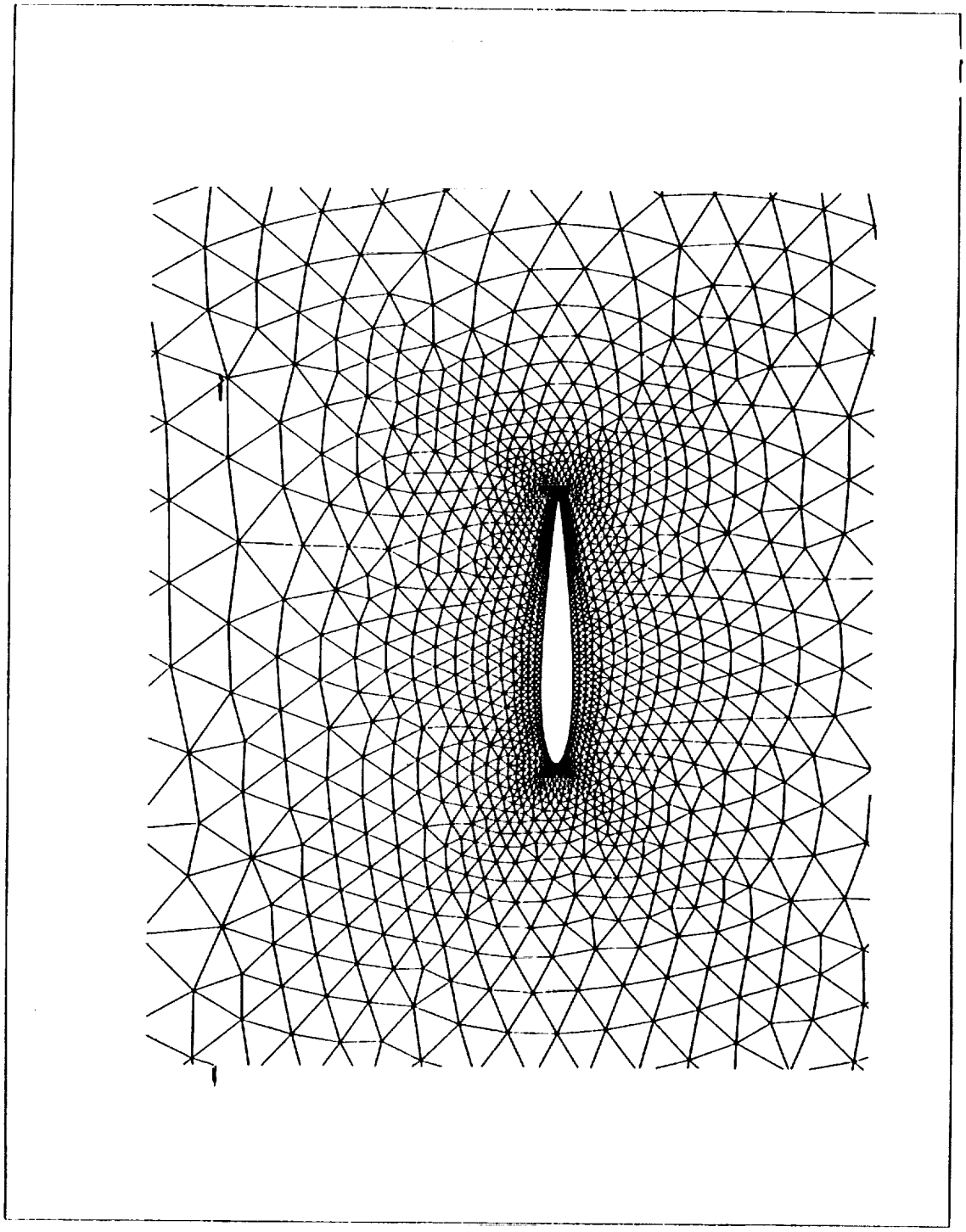

Fig. 4.12 Adapted grid for NACA 0012 airfoil.

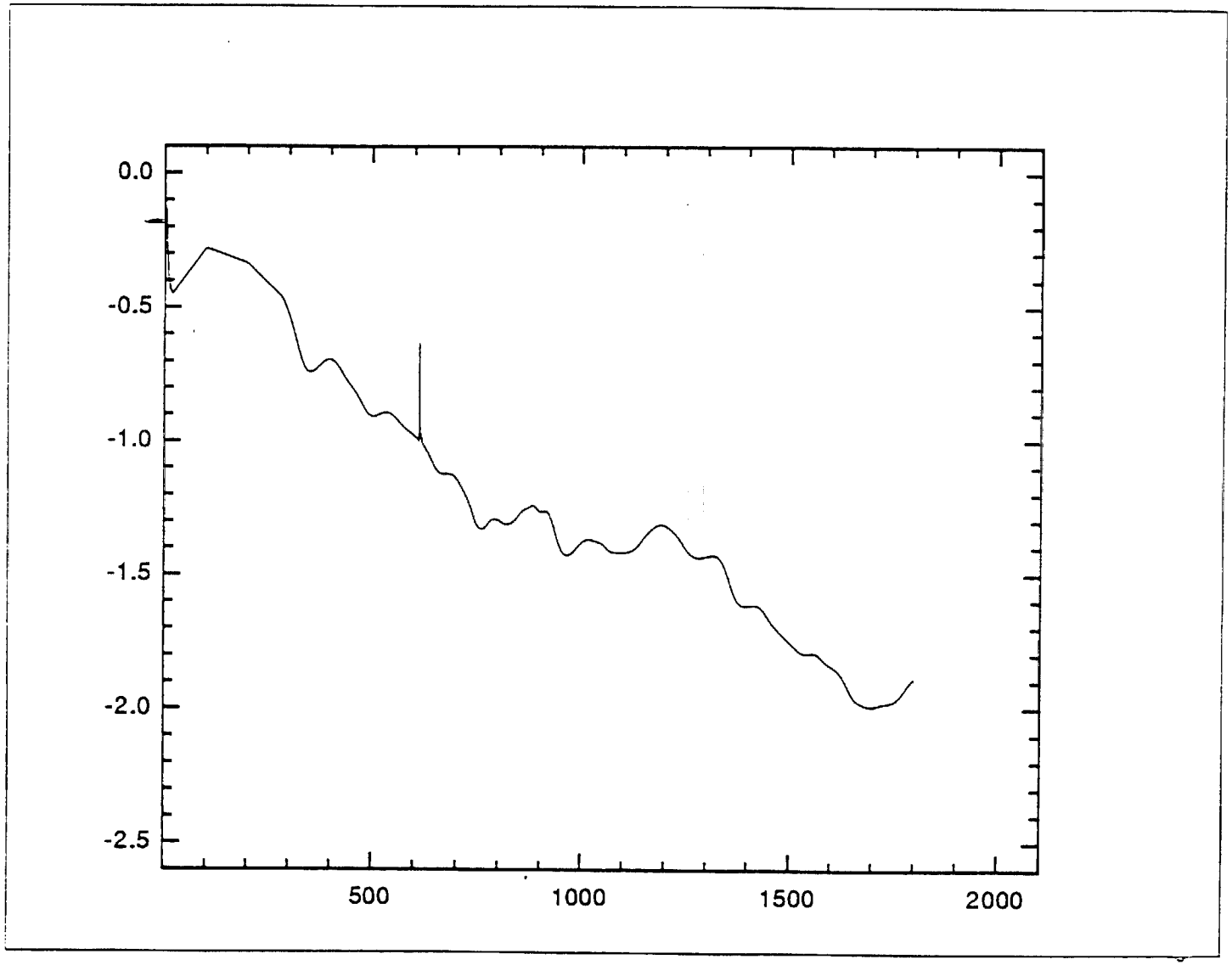

Fig. 4.13 Convergence history with initial free stream conditions.

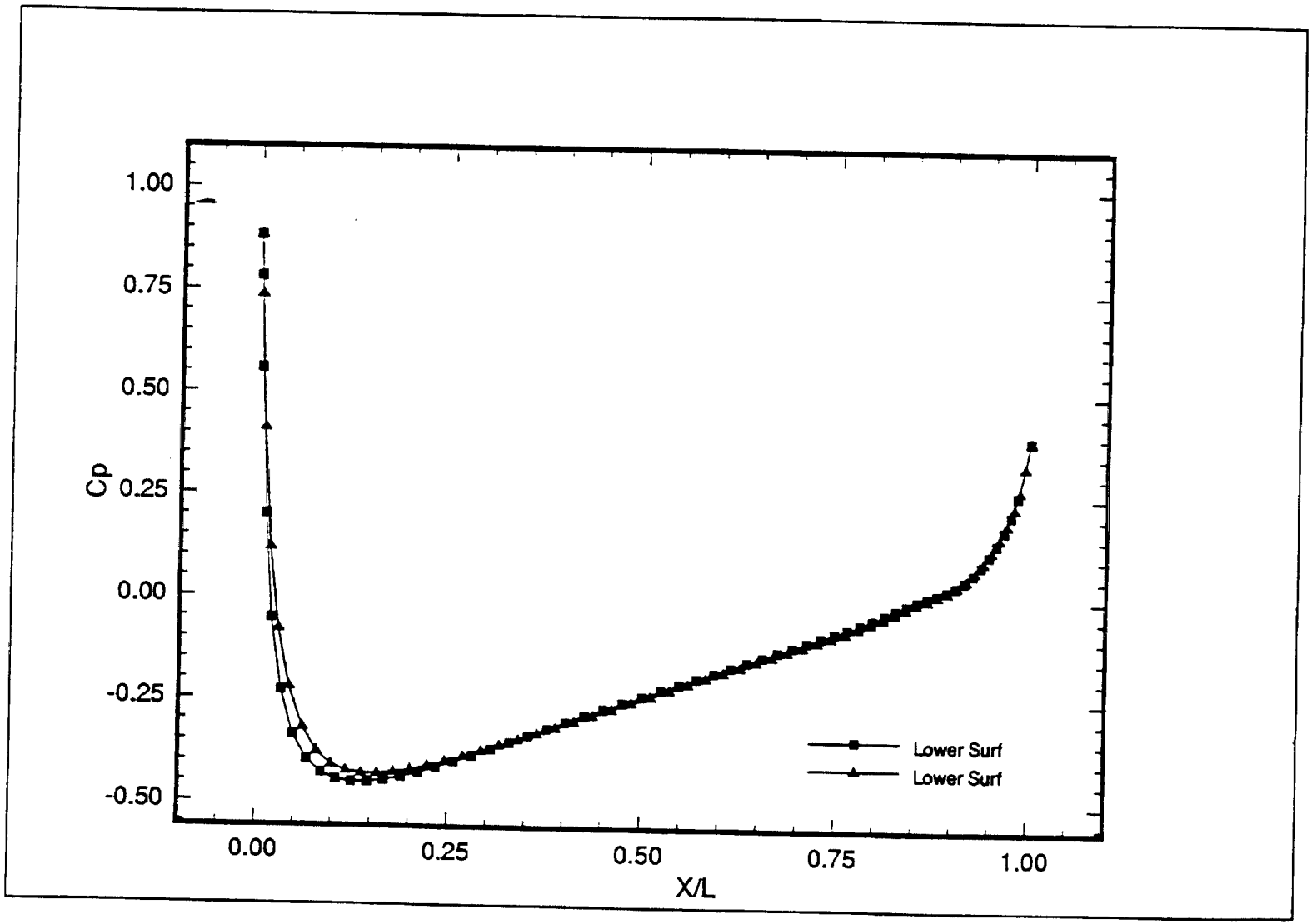

Fig. 4.14 Mach number contours for the adapted grid.

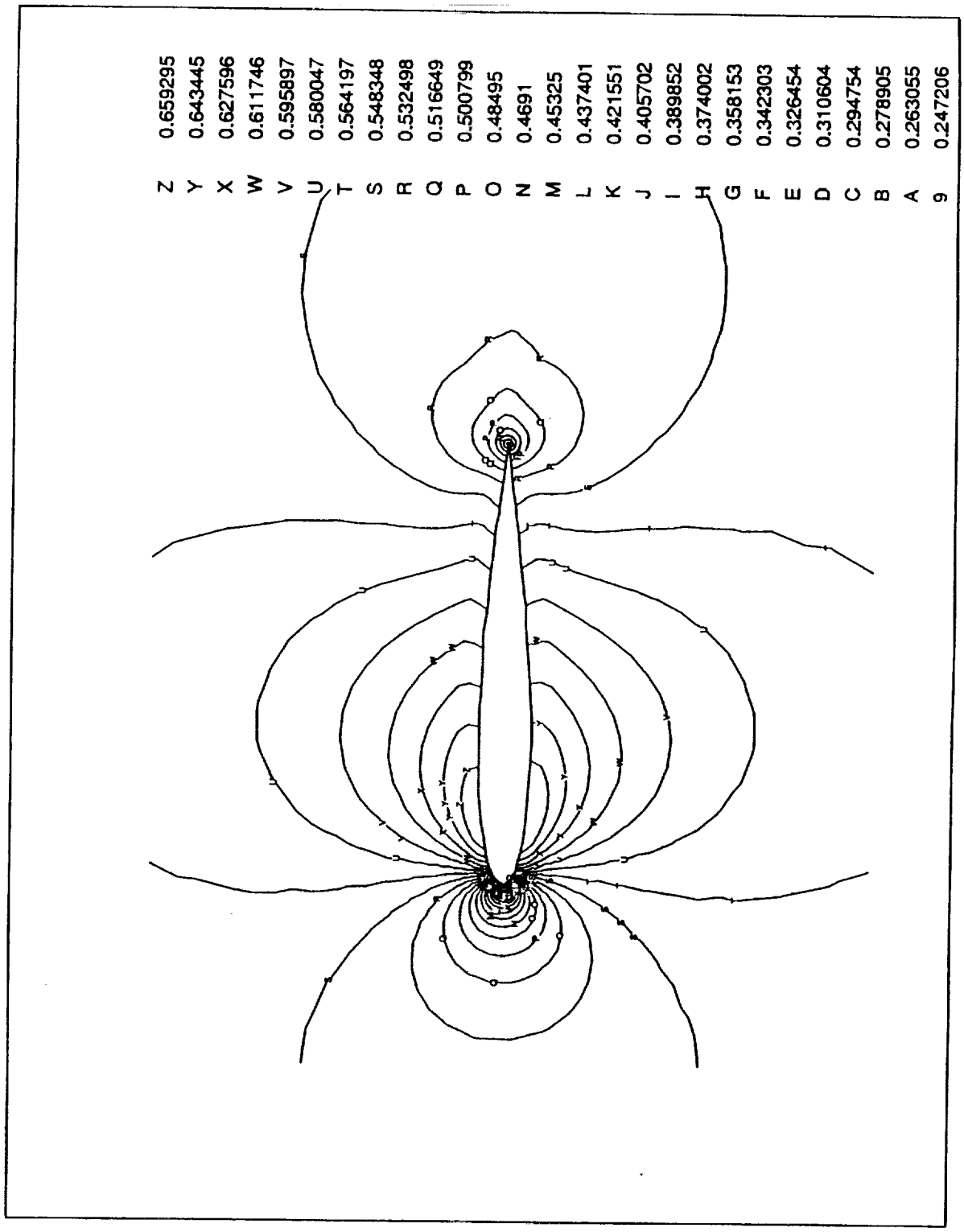

Fig. 4.15 Variation of coefficient of pressure over the upper and lower surface.

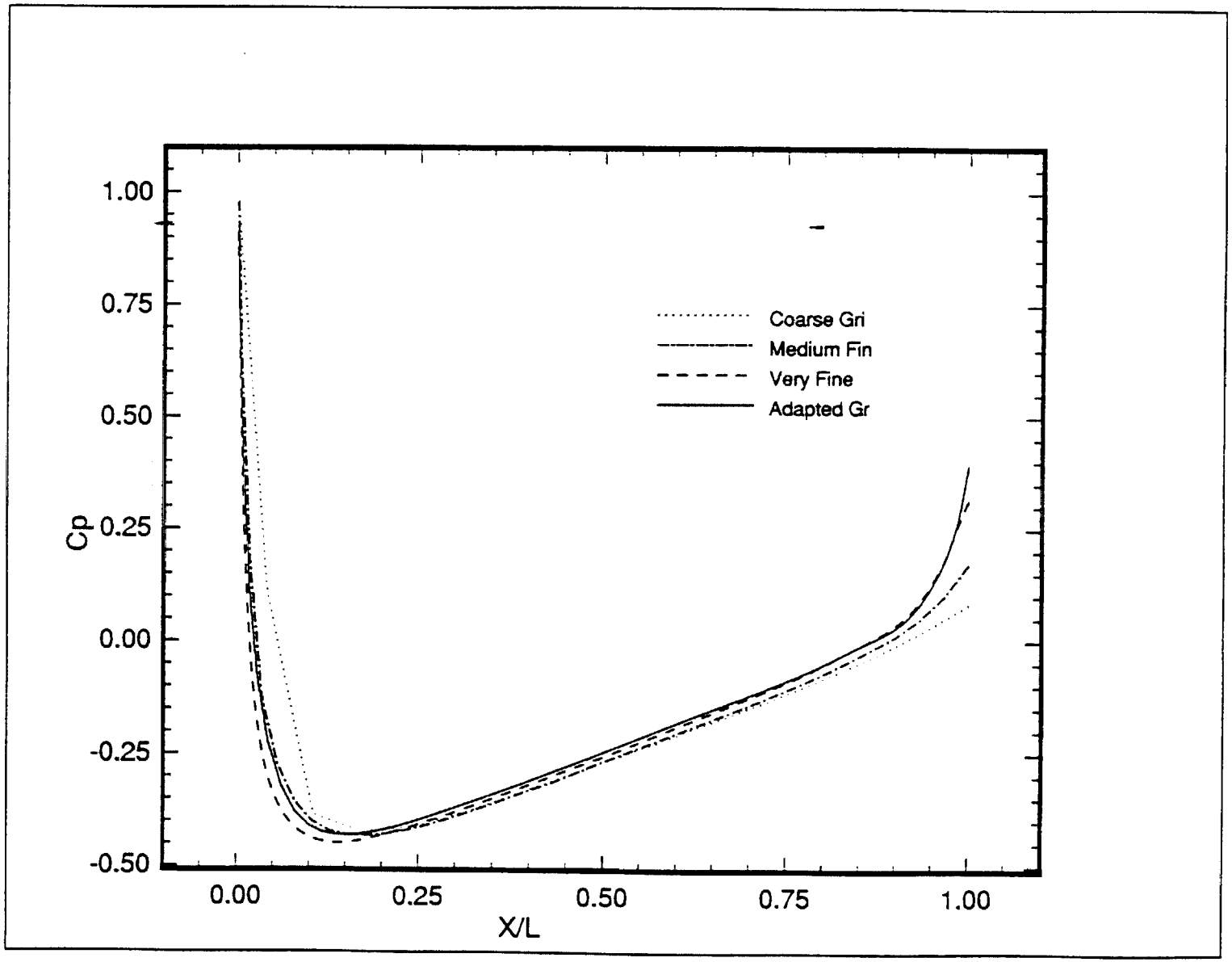

Fig. 4.16 Comparison of Cp on the upper surface for four different grid concentration.

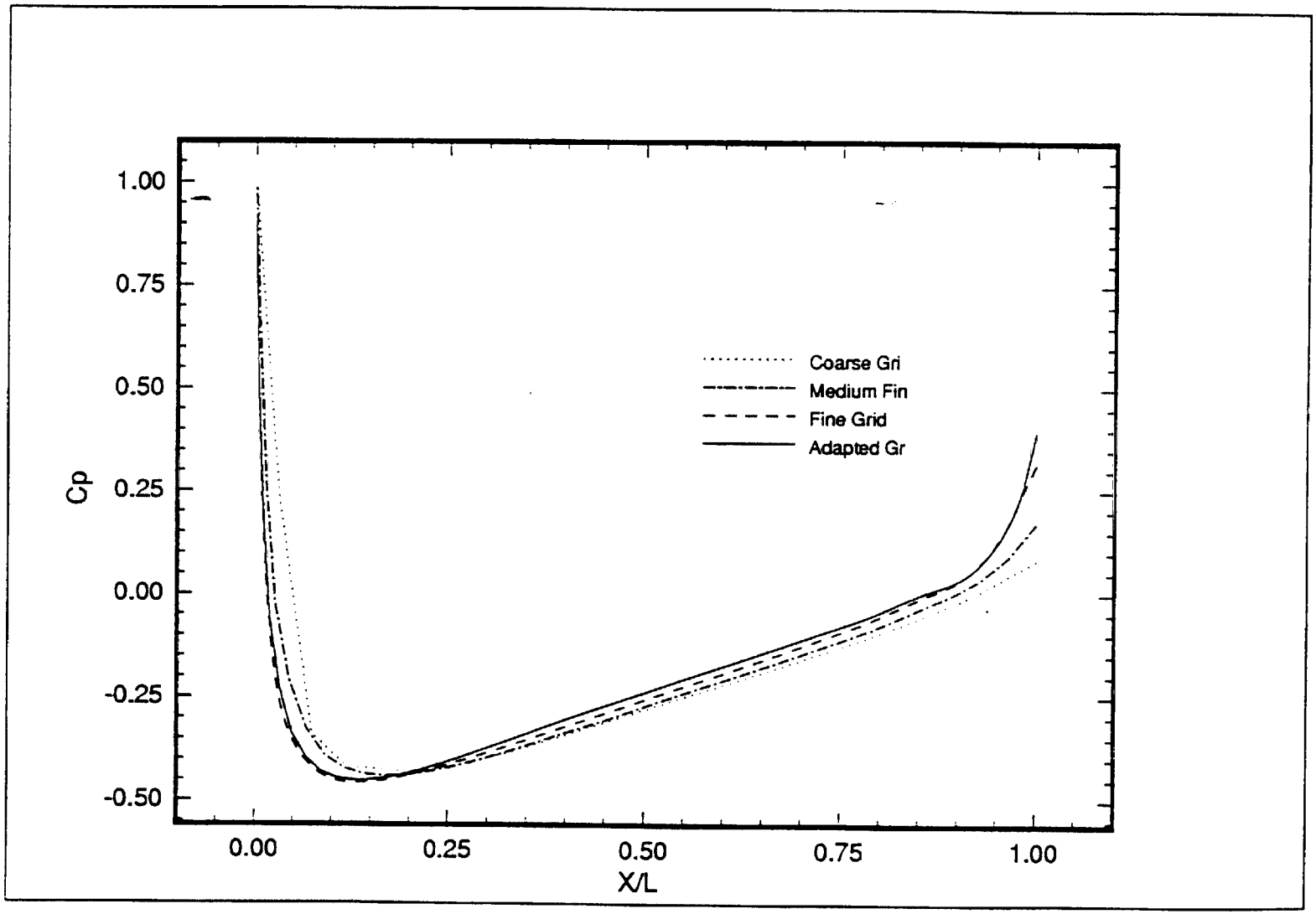

Fig. 4.17 Comparison of Cp on the lower surface for four different grid concentration.

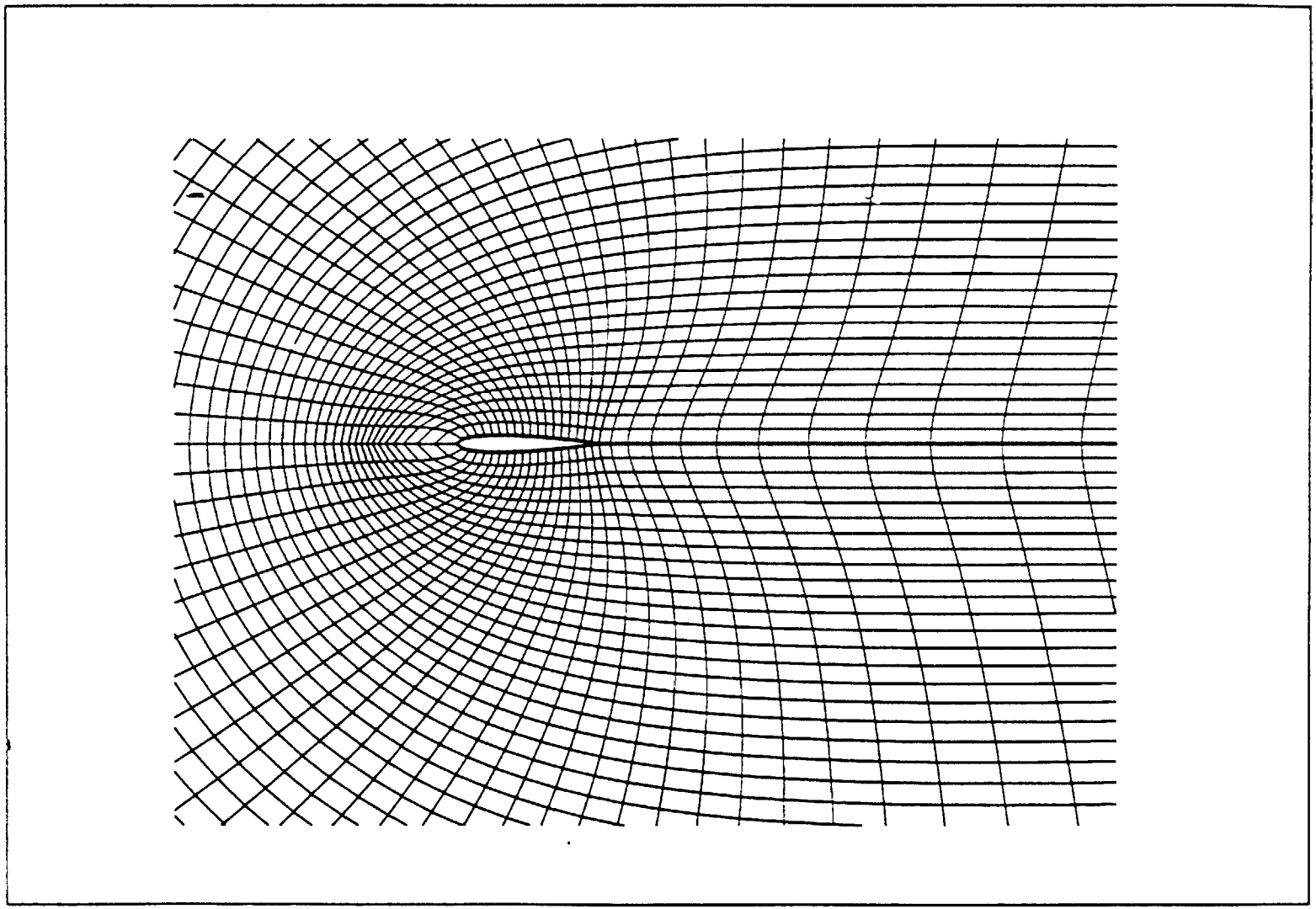

Fig. 4.18 Initial coarse structured grid for NACA 0012 airfoil.

Figure 4.18 shows the coarse grid with 38 points around the airfoil and 49 points in the normal direction. Figure 4.19 shows the Mach number contour plot and Fig. 4.20 the Cp distribution. Both figures show the symmetric distribution of the flow field quantities. The Cp values for the top and bottom surfaces exactly match each other. Figure 4.21 shows the comparison of Cp between structured and unstructured grids. Near the stagnation point, the unstructured grid predicts the flow accurately but the structured grid gives a poor result. This might be due to the coarse distribution of the grid points near the leading edge.

To investigate the leading edge inaccuracy, a medium fine grid is selected with the same number of grid points as in the unstructured grid i.e., 76 points. Figure 4.22 shows the grid distribution. Computations were performed with free stream initial conditions, and Mach number contours for a steady state solution are plotted in Fig. 4.23. Again, a symmetric distribution of flow field quantities is seen. The Cp plot is shown in Fig. 4.24 and Fig. 4.25 shows the comparison with the unstructured grid. A better prediction of the flow field quantities is seen near the leading edge.

Next, a very fine grid with 163 points around the surface of the airfoil is generated. In this case also the solution was started with the free stream initial condition. Figure 4.26 shows the grid distribution and Fig. 4.27 the Mach number contour plot. Coefficient of pressure for the top and bottom surface is shown in Fig. 4.28. The flow field is symmetrical and a very good estimation of the flow field quantities is seen near the leading edge. Figure 4.29 shows the Cp comparison with the unstructured grid and Fig. 4.30 shows the comparison of Cp for different grid concentration. It is seen that as the grid is concentrated around the airfoil better results are obtained. Coefficient of pressure distribution along the surface for both structured and unstructured grid is compared with the experimental values obtained by Harris [9] in Fig. 4.31.

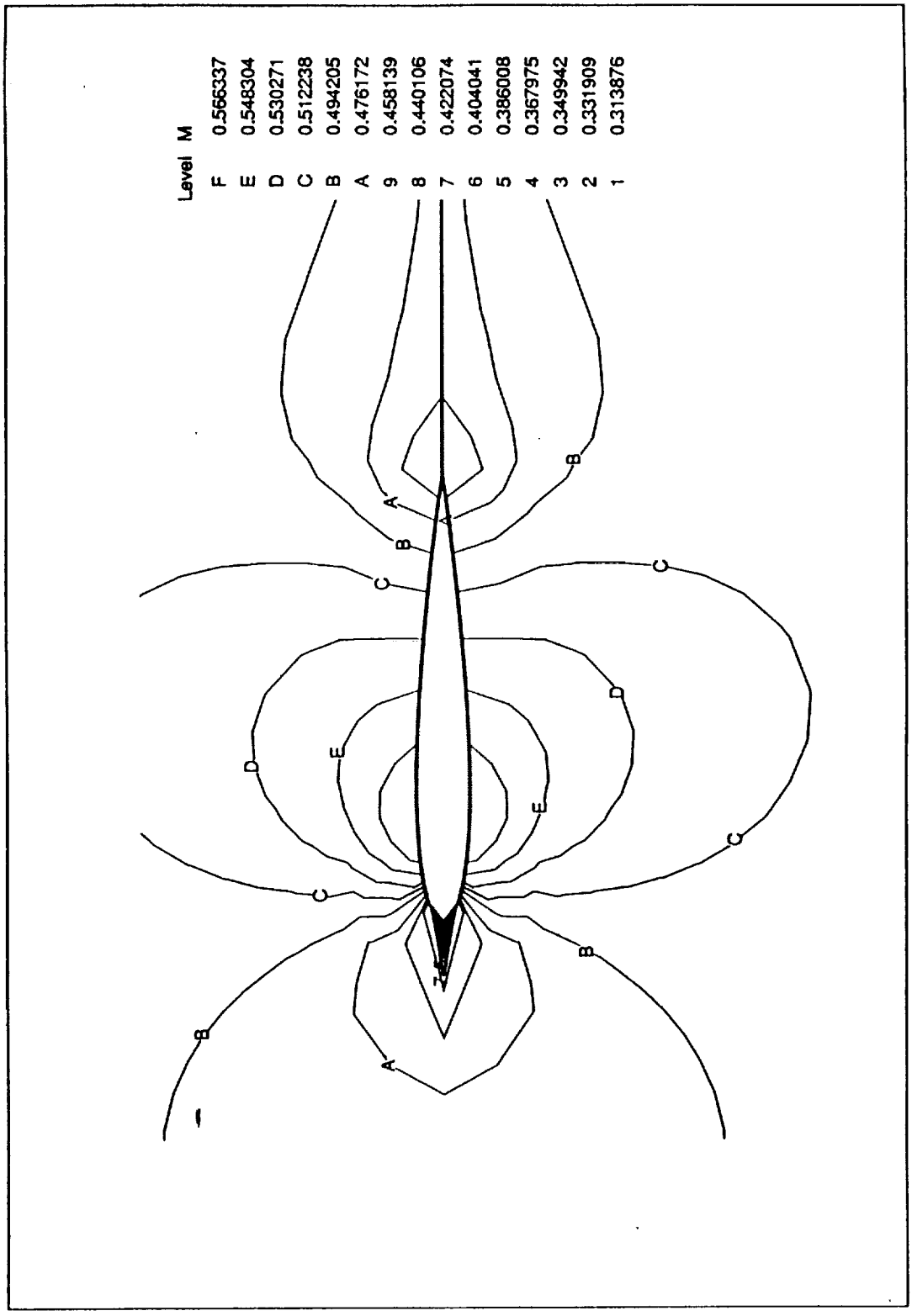

Fig. 4.19 Mach number contours for the coarse grid.

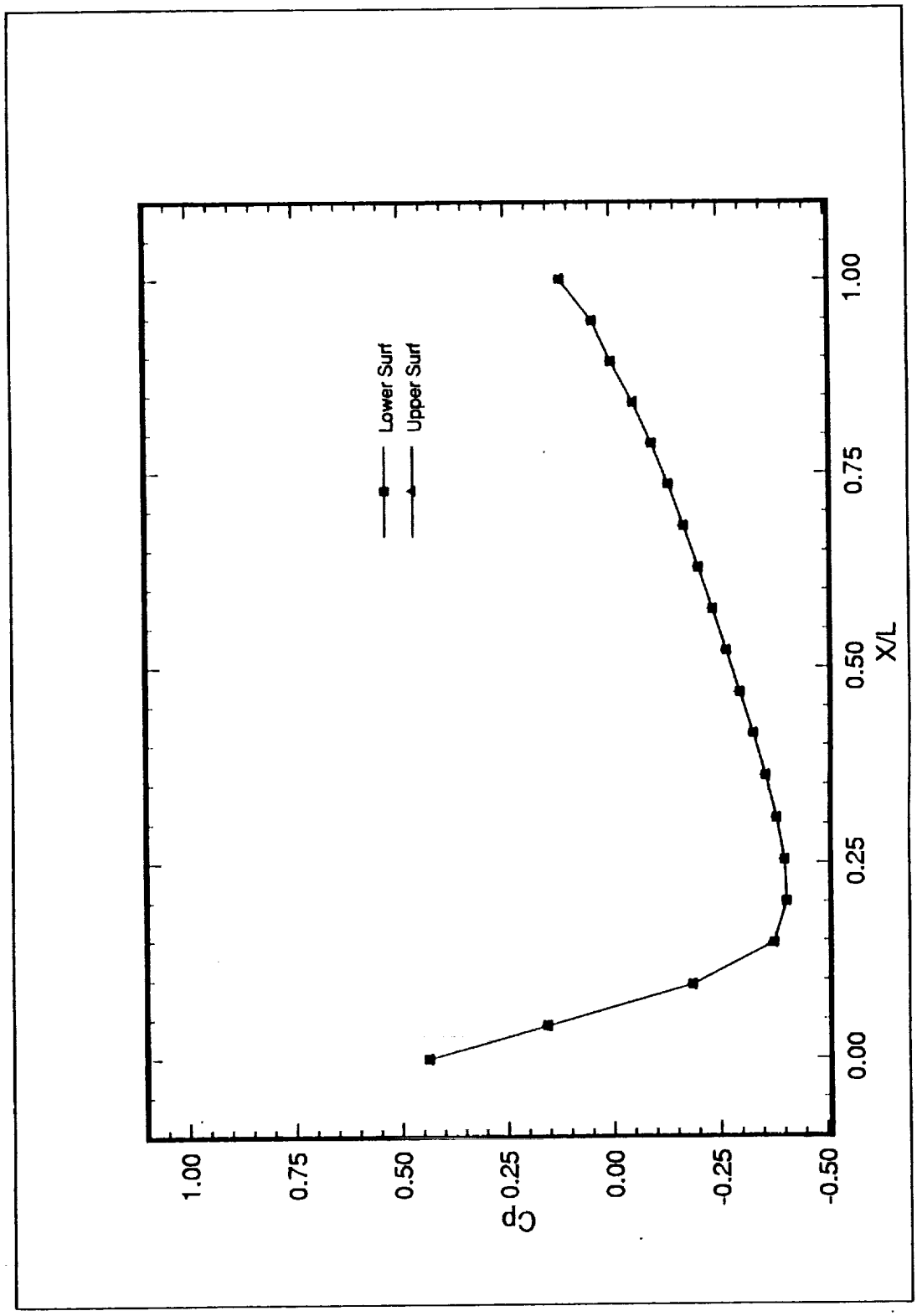

Fig. 4.20 Variation of coefficient of pressure over the upper and lower surface.

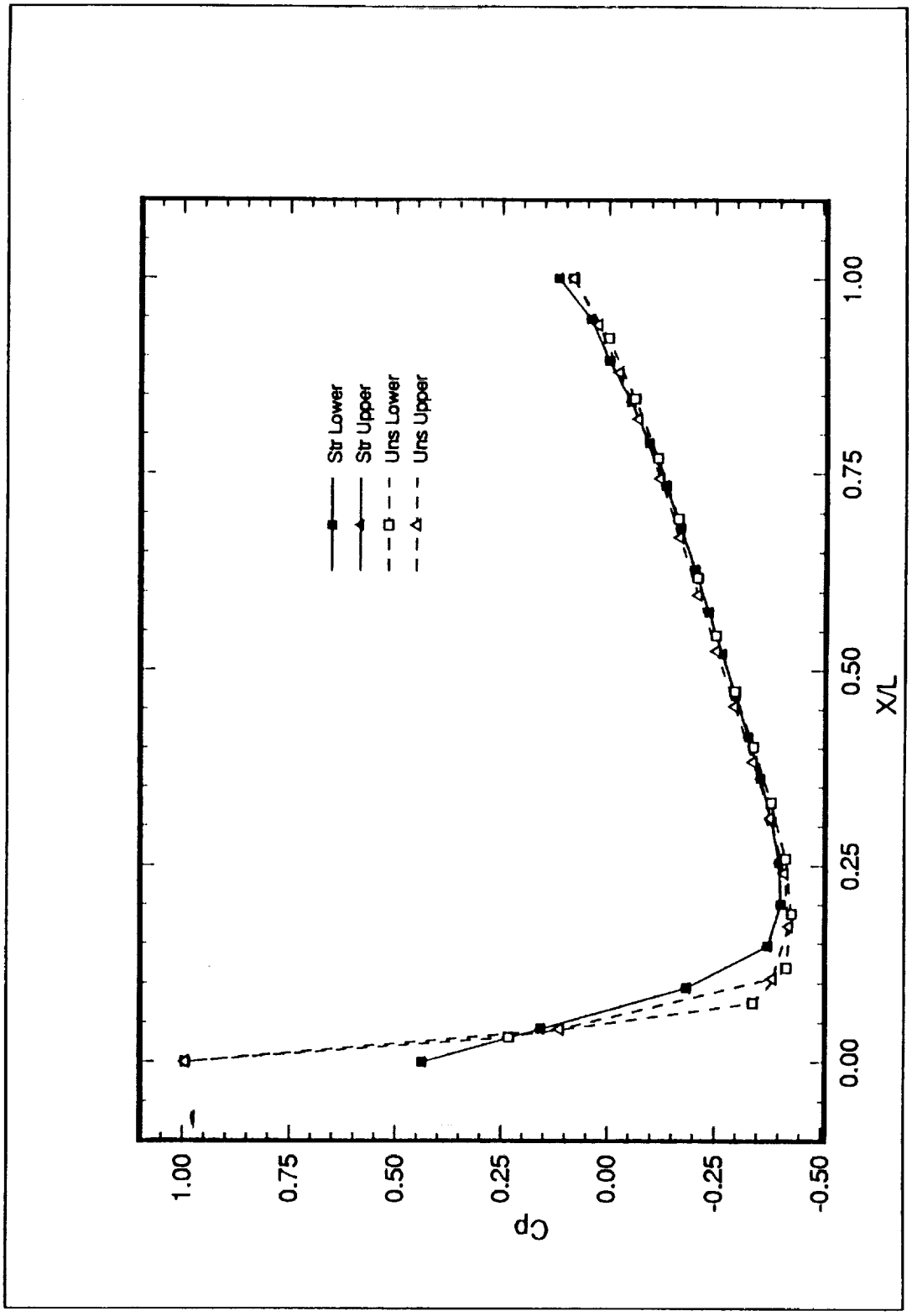

Fig. 4.21 Comparison of Cp between lower and upper surface.

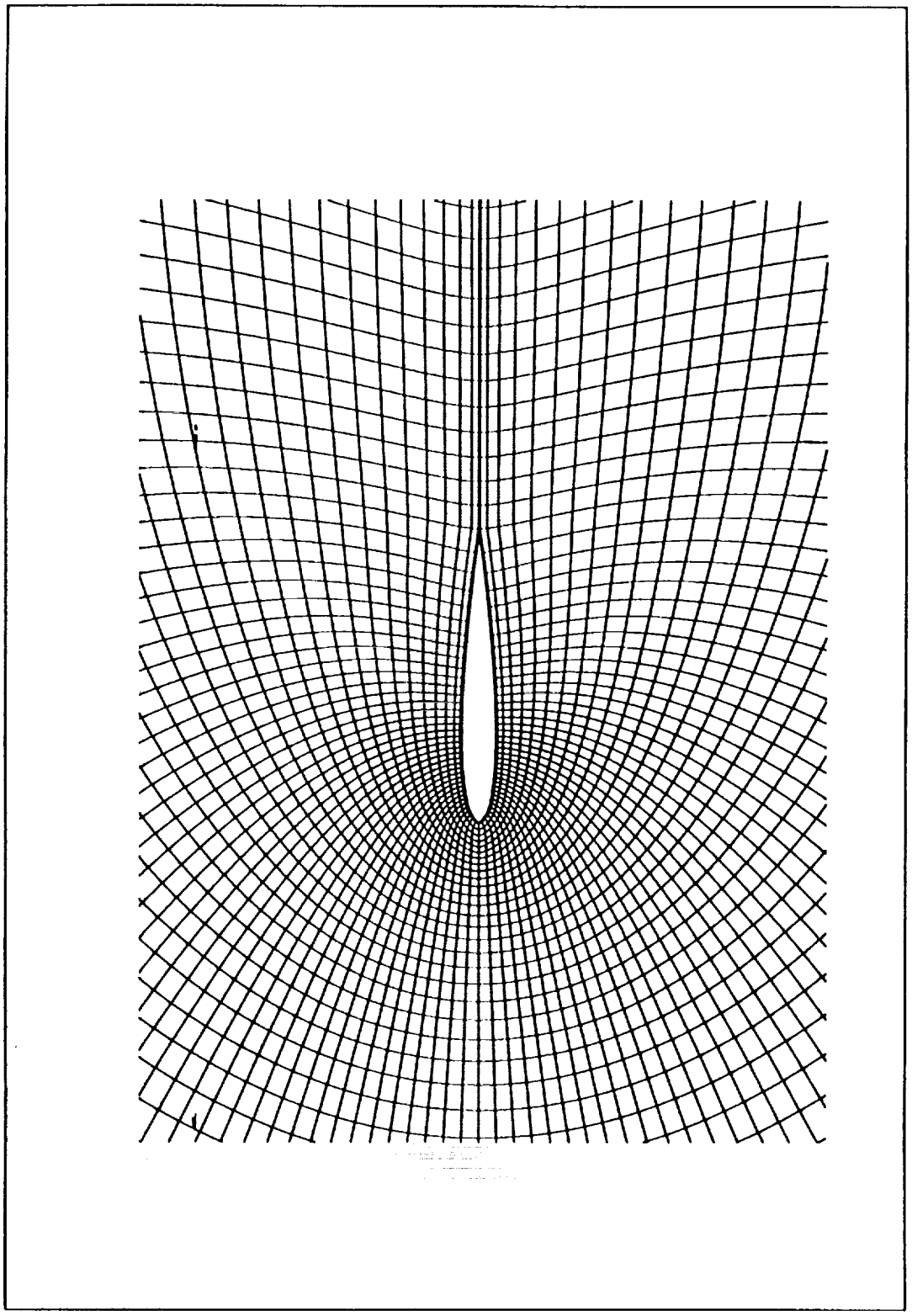

Fig. 4.22 Medium fine grid for NACA 0012 airfoil.

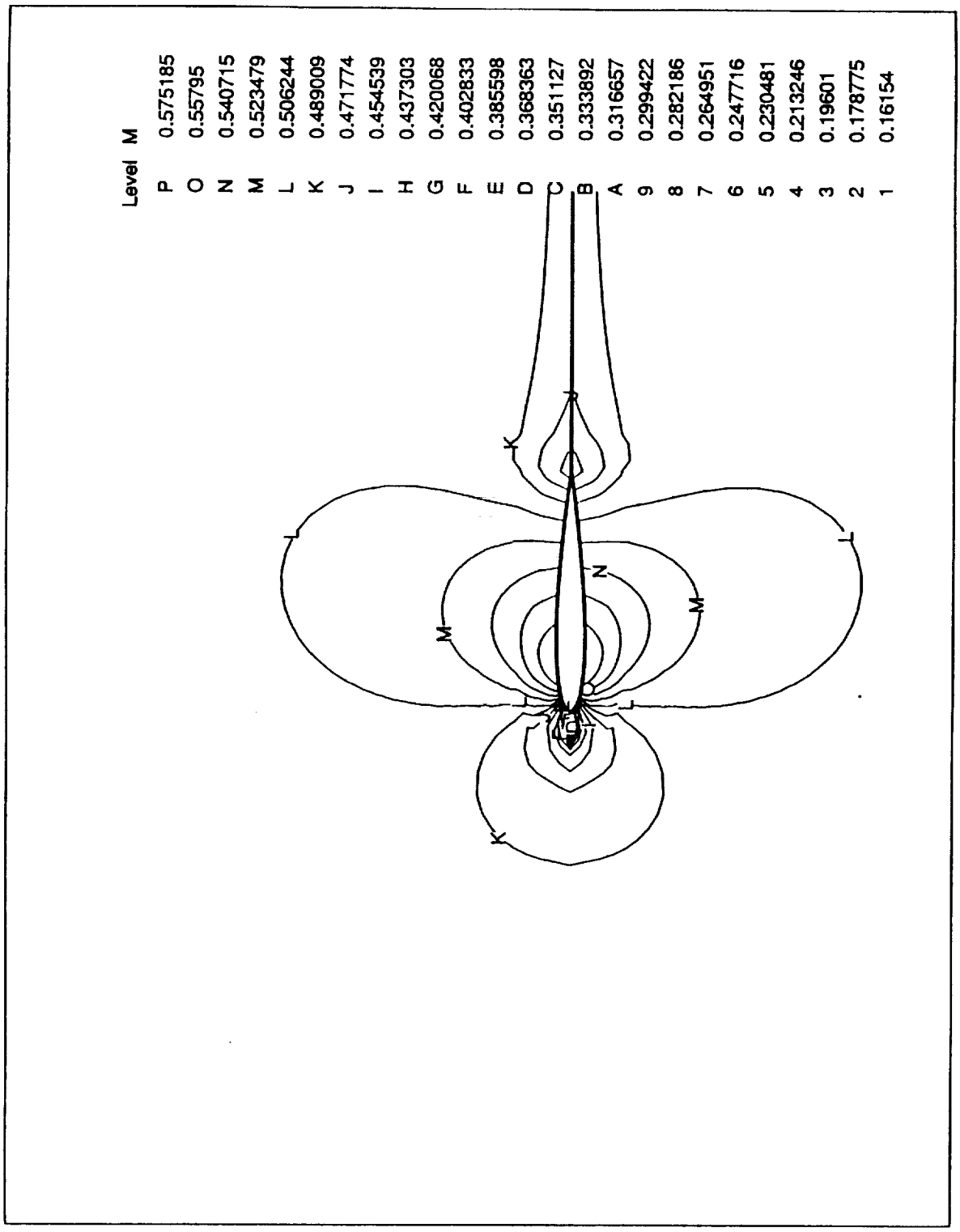

Fig. 4.23 Mach number contours for medium grid.

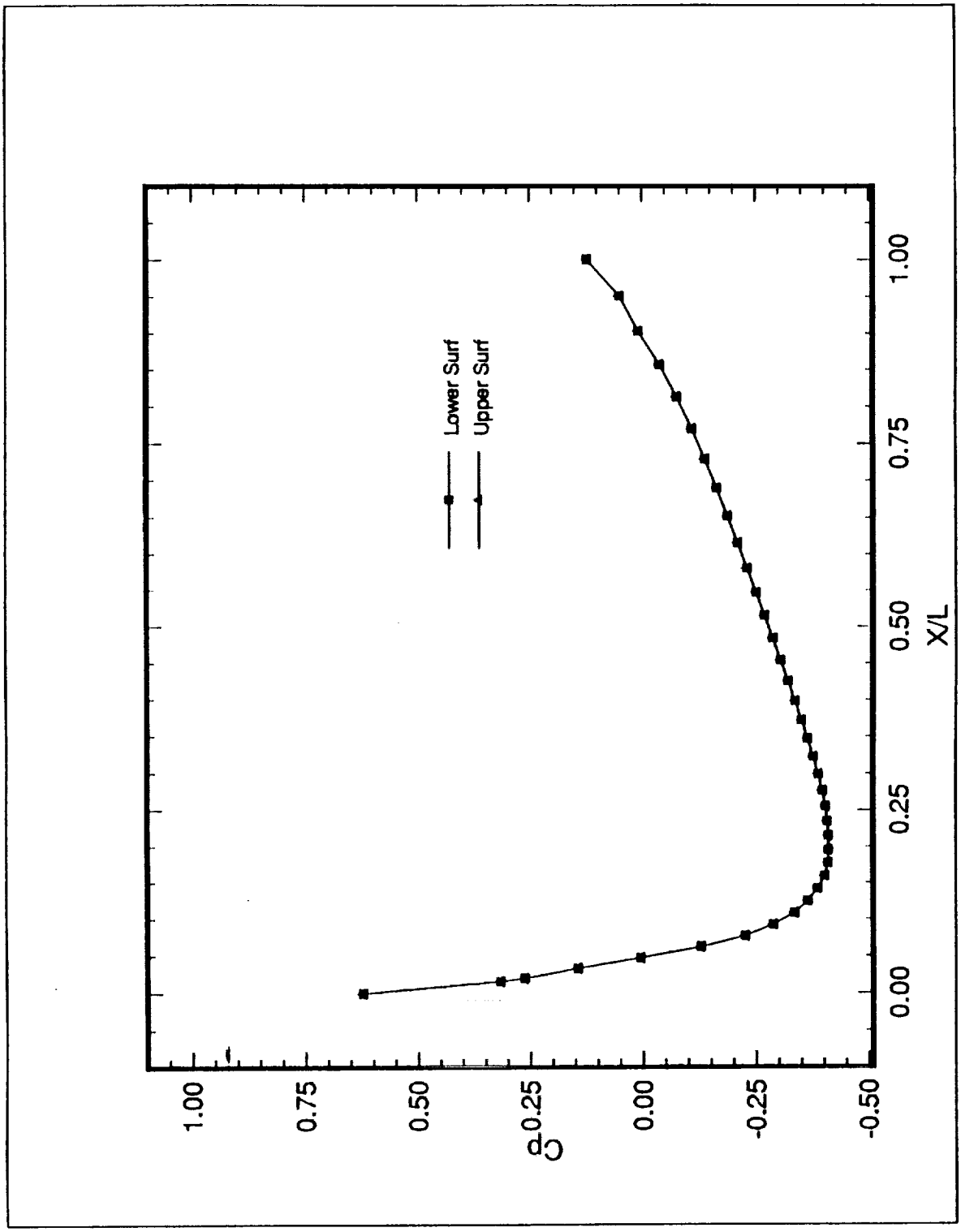

Fig. 4.24 Variation of coefficient of pressure over the upper and lower surface.

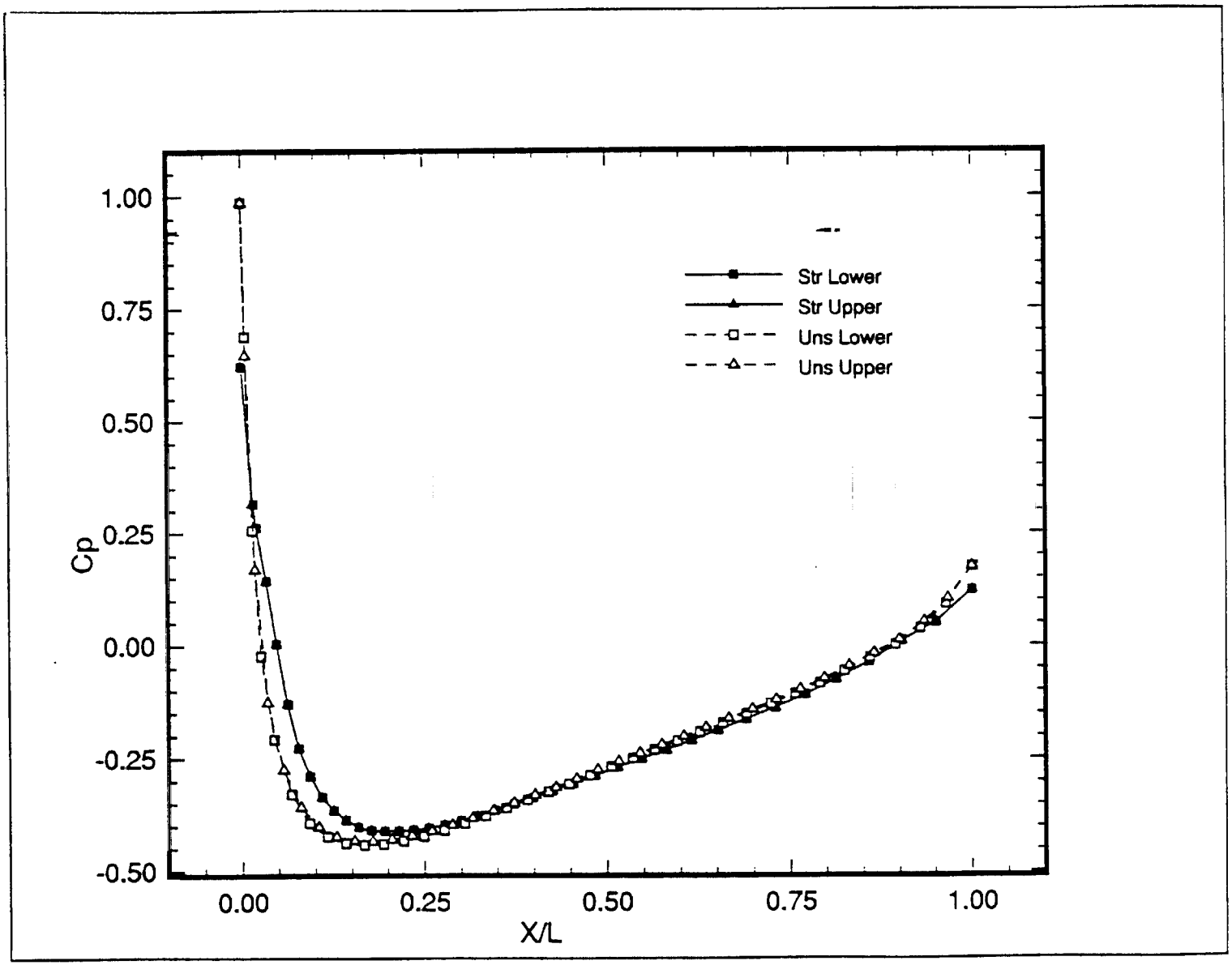

Fig. 4.25 Comparison of Cp between structured and unstructured grid.

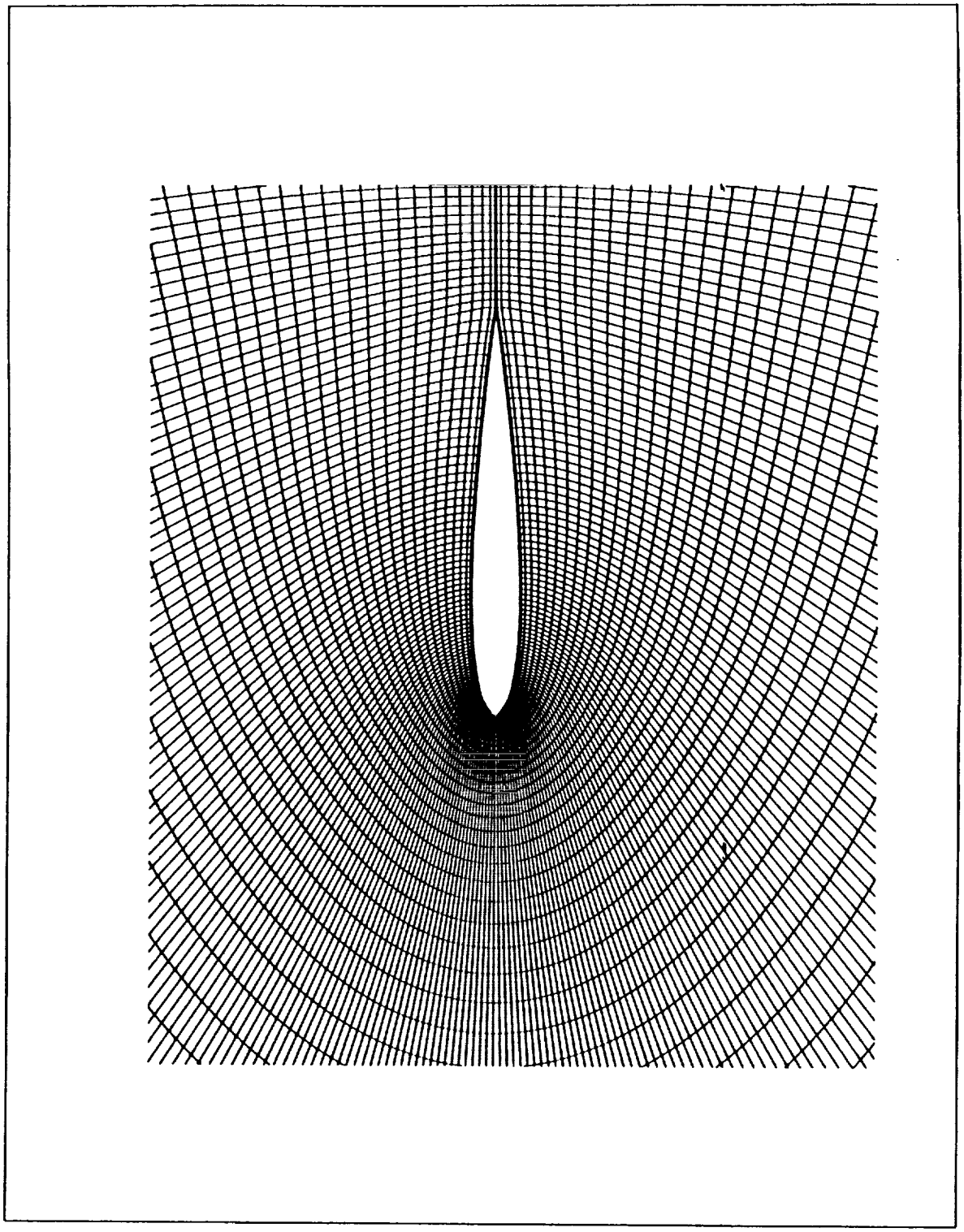

Fig. 4.26 Fine grid for NACA 0012 airfoil.

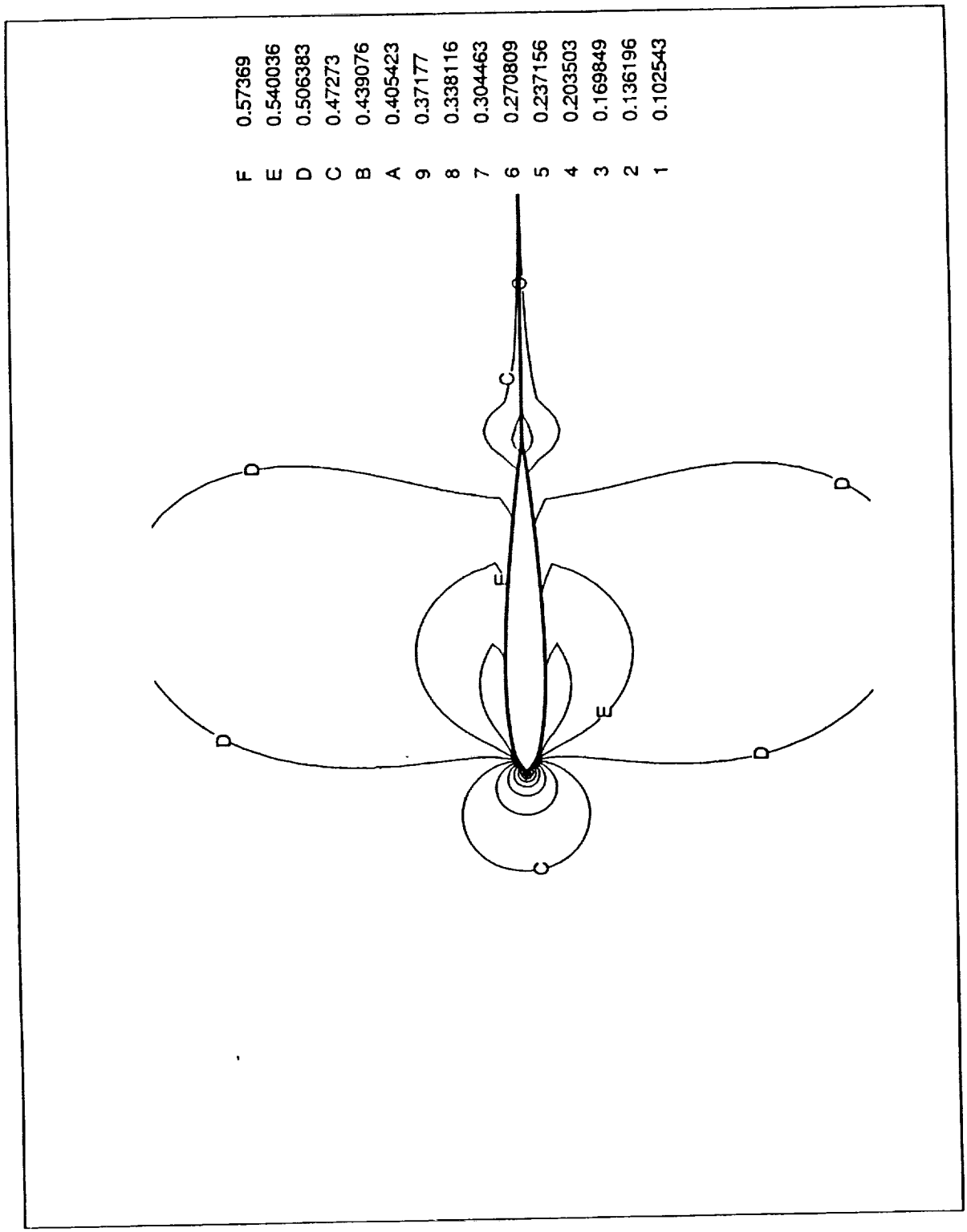

Fig. 4.27 Mach number contours for fine grid.

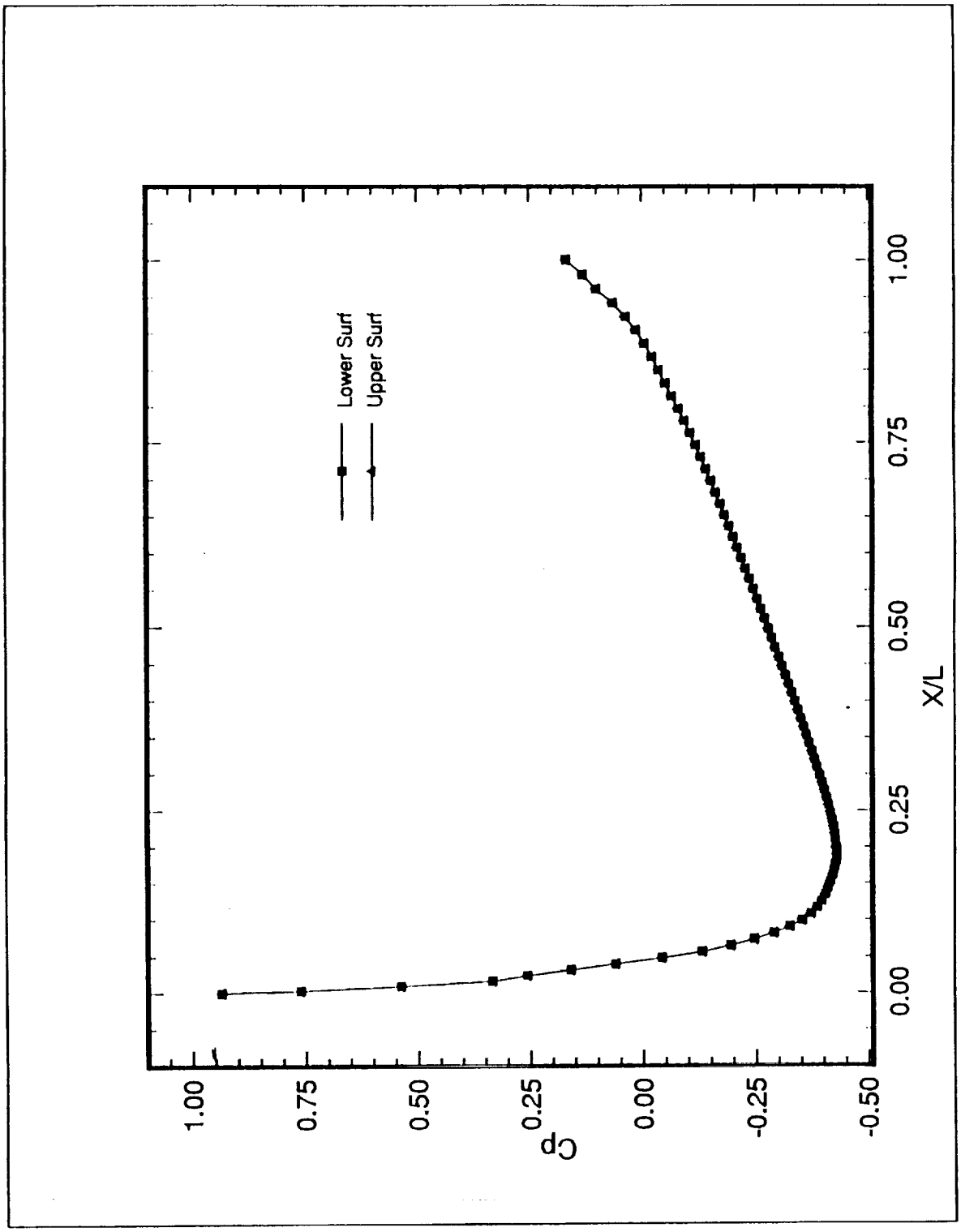

Fig. 4.28 Variation of coefficient of pressure over the upper and lower surface.

Its seen that the structured grid has a much better agreement with the experimental values than unstructured grid. This might be due to the efficient flow solver used for structured grid than the unstructured grid.

Comparison between the structured and unstructured grid for the various grid concentration is shown in Table 1. The table also shows the percentage of error in pressure calculated at the stagnation point. It is seen from the table that structured grid requires more number of points to accurately predict the flow field when compared to unstructured grid.

Case 3

In this case the same airfoil was considered as in case 1 but for a Mach number of 0.84 and 1.25° angle of attack. Figures 4.32 and 4.33 show the Mach number and pressure contours. Here, a shock in the form of an expansion wave is observed over the top surface and a compression wave at the bottom surface. Figure 4.34 shows the coefficient of pressure plotted over the upper and lower surface. For this case the lift and drag coefficient were computed to be C_l = 0.07, C_d = 0.02

Case 4

In this test case a biplane is considered made up of two NACA 0012 airfoils. The outer boundaries are located at a distance of ten chord lengths. The distance between the two airfoils is one chord length with the top airfoil shifted from the center by 0.5 chord lengths. The grid for this case is shown in fig. 4.35. The above geometry was tested for a Mach Number of 0.8

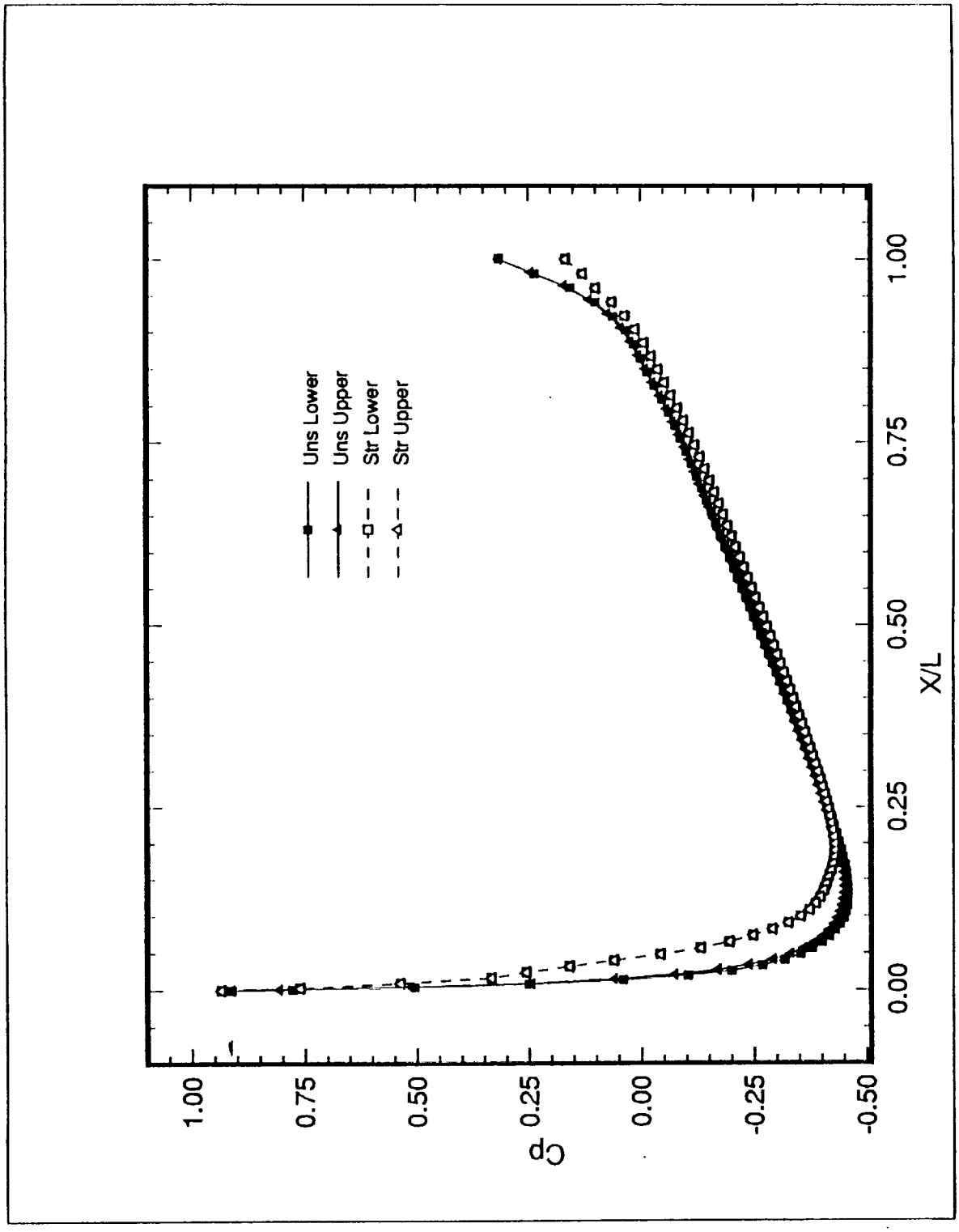

Fig. 4.29 Comparison of Cp between structured and unstructured grid for a fine mesh.

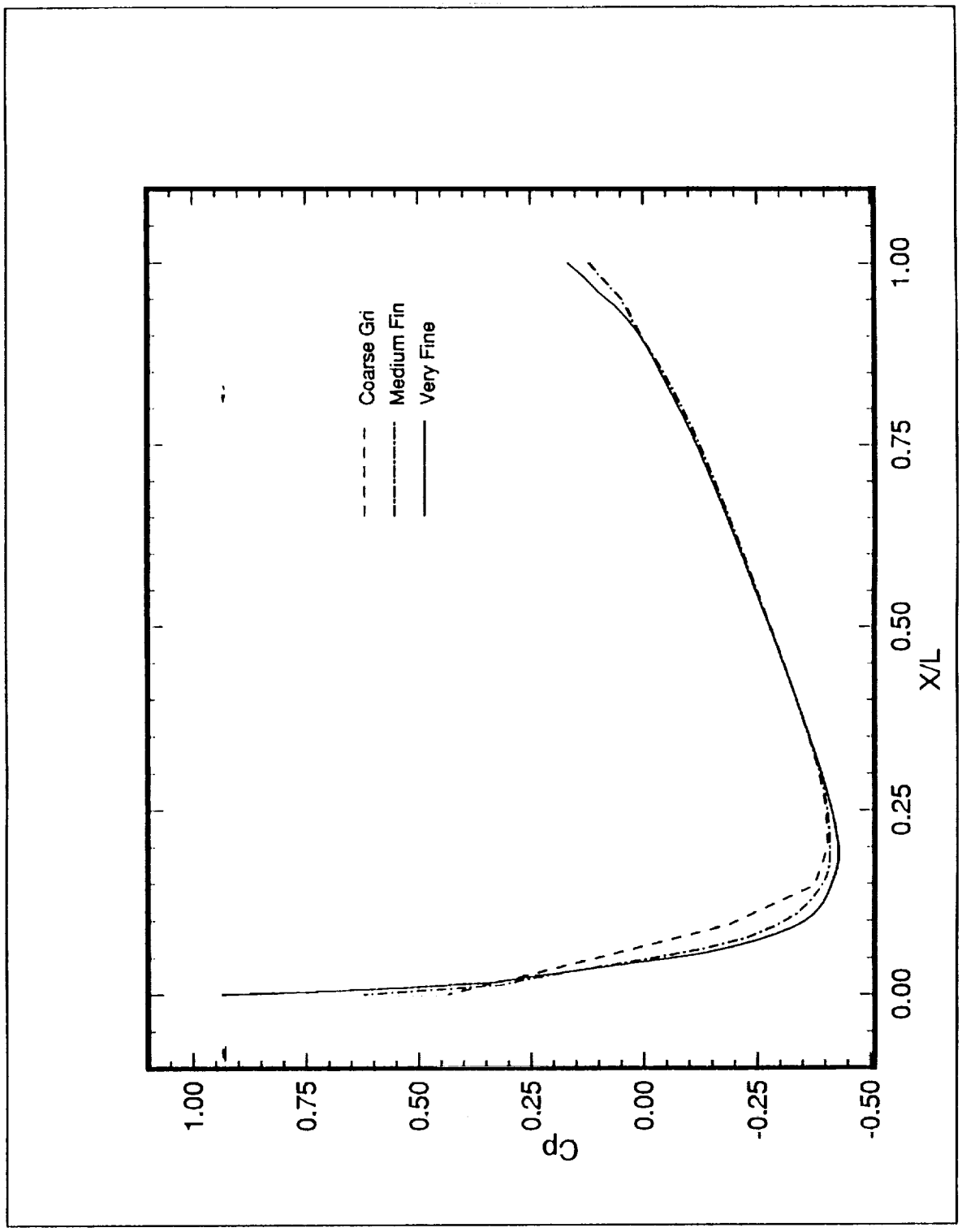

Fig. 4.30 Comparison of Cp for three different grid concentration.

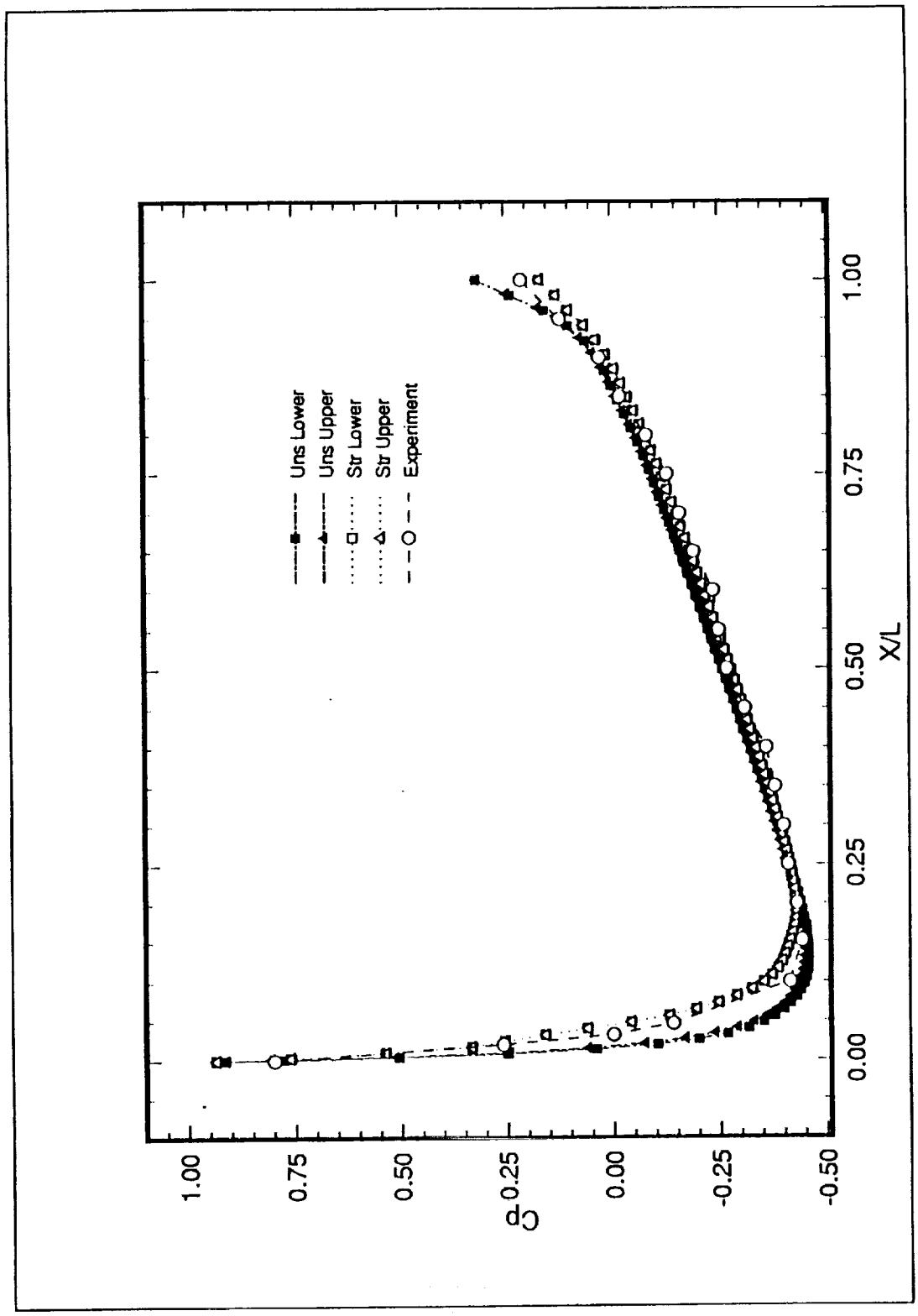

Fig. 4.31 Comparison of Cp with experimental values.

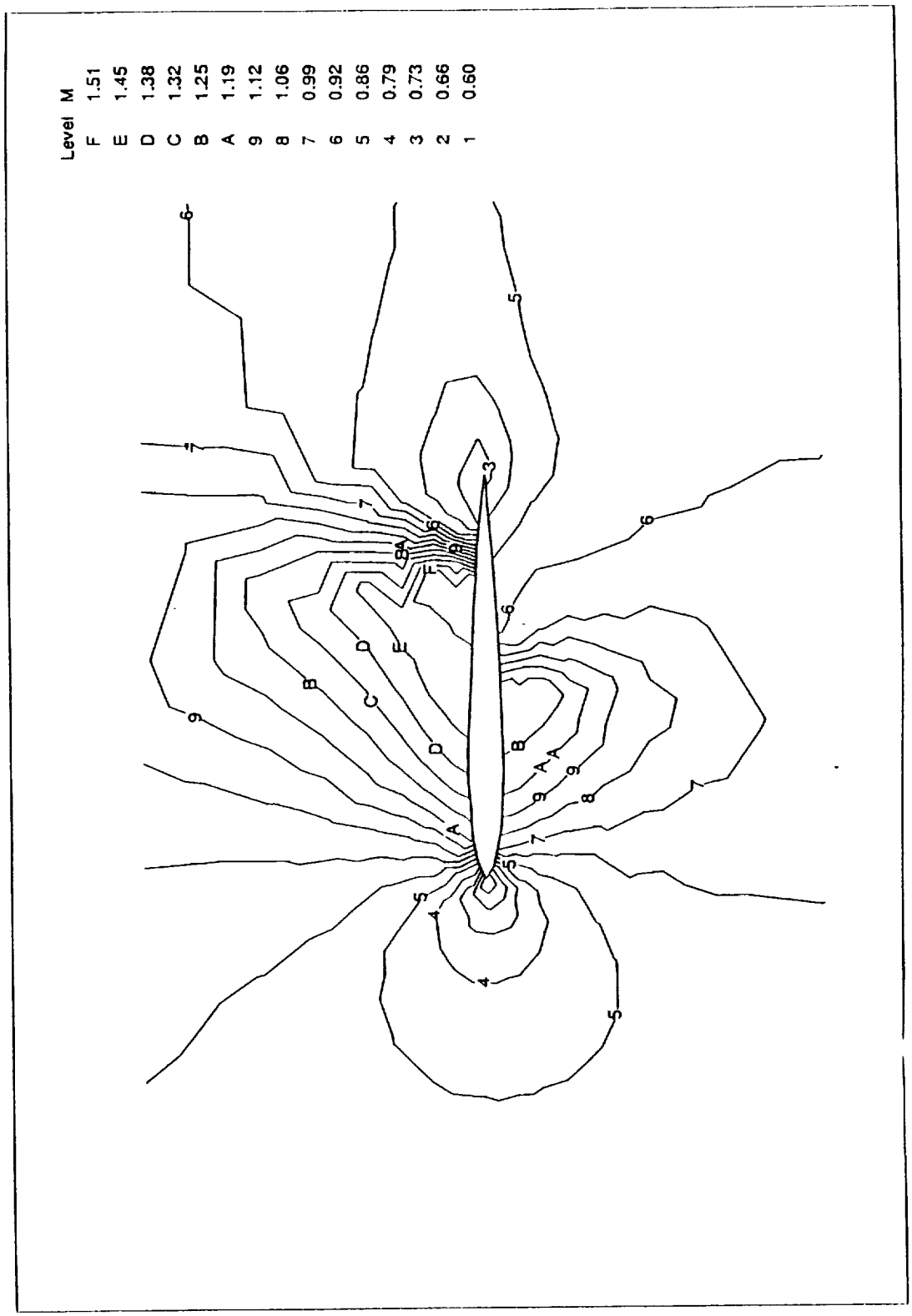

Fig. 4.32 Mach number contours for NACA 0012 airfoil ($M_\infty = 0.84$, $\alpha = 1.25$).

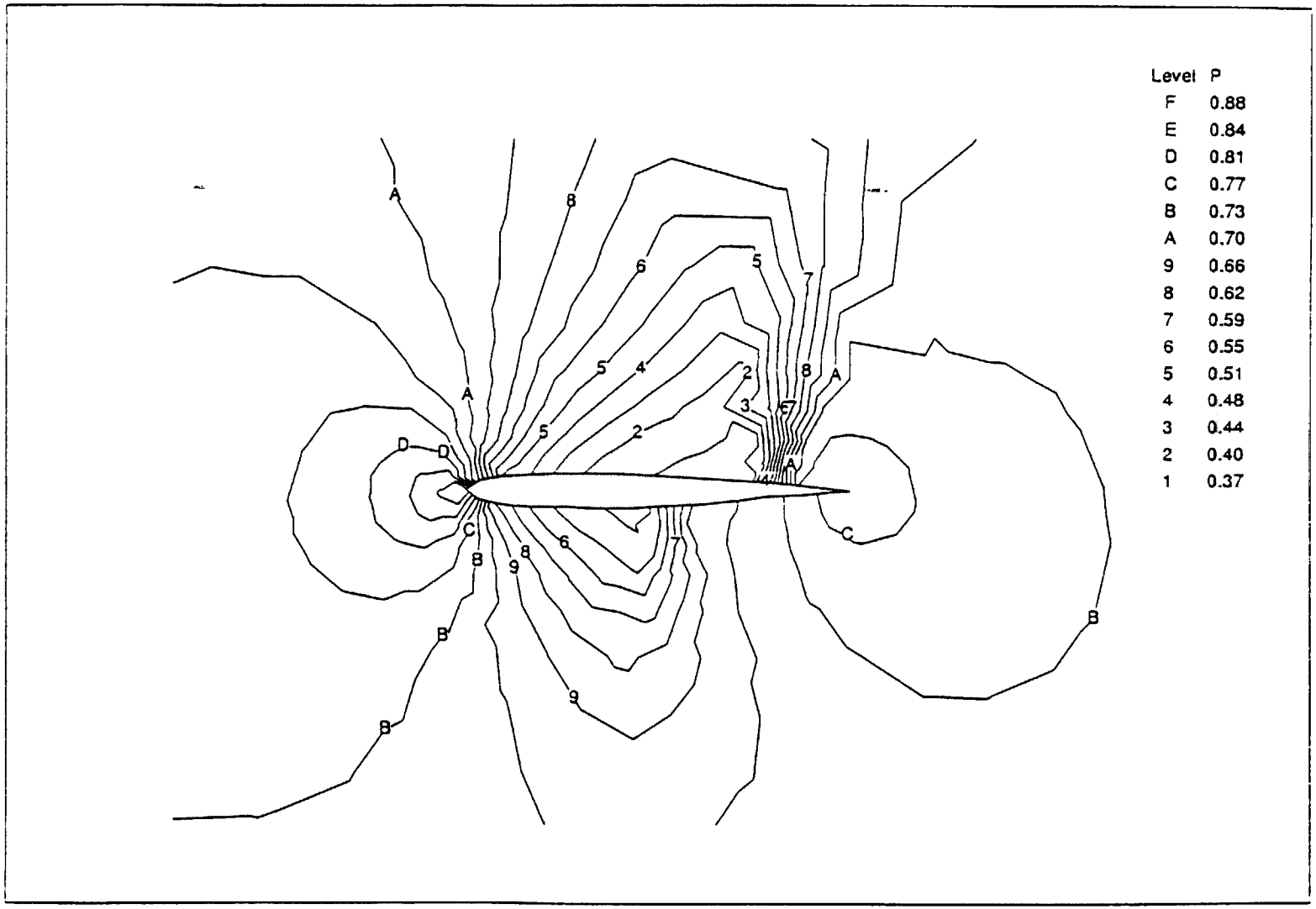

Fig. 4.33 Pressure contours for NACA 0012 airfoil ($M_\infty = 0.84$, $\alpha = 1.25$).

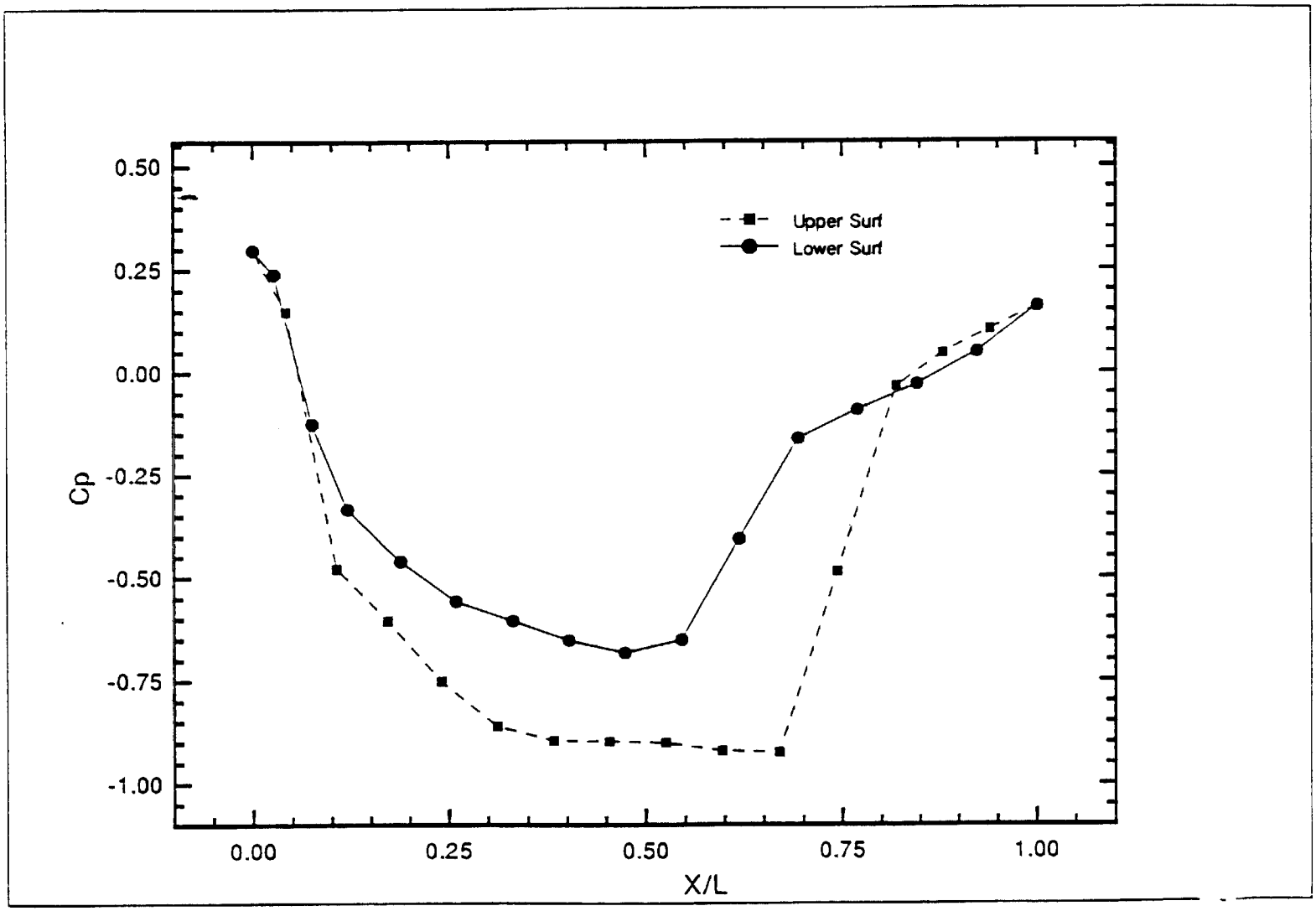

Fig. 4.34 Variation of pressure over the upper and lower surface.

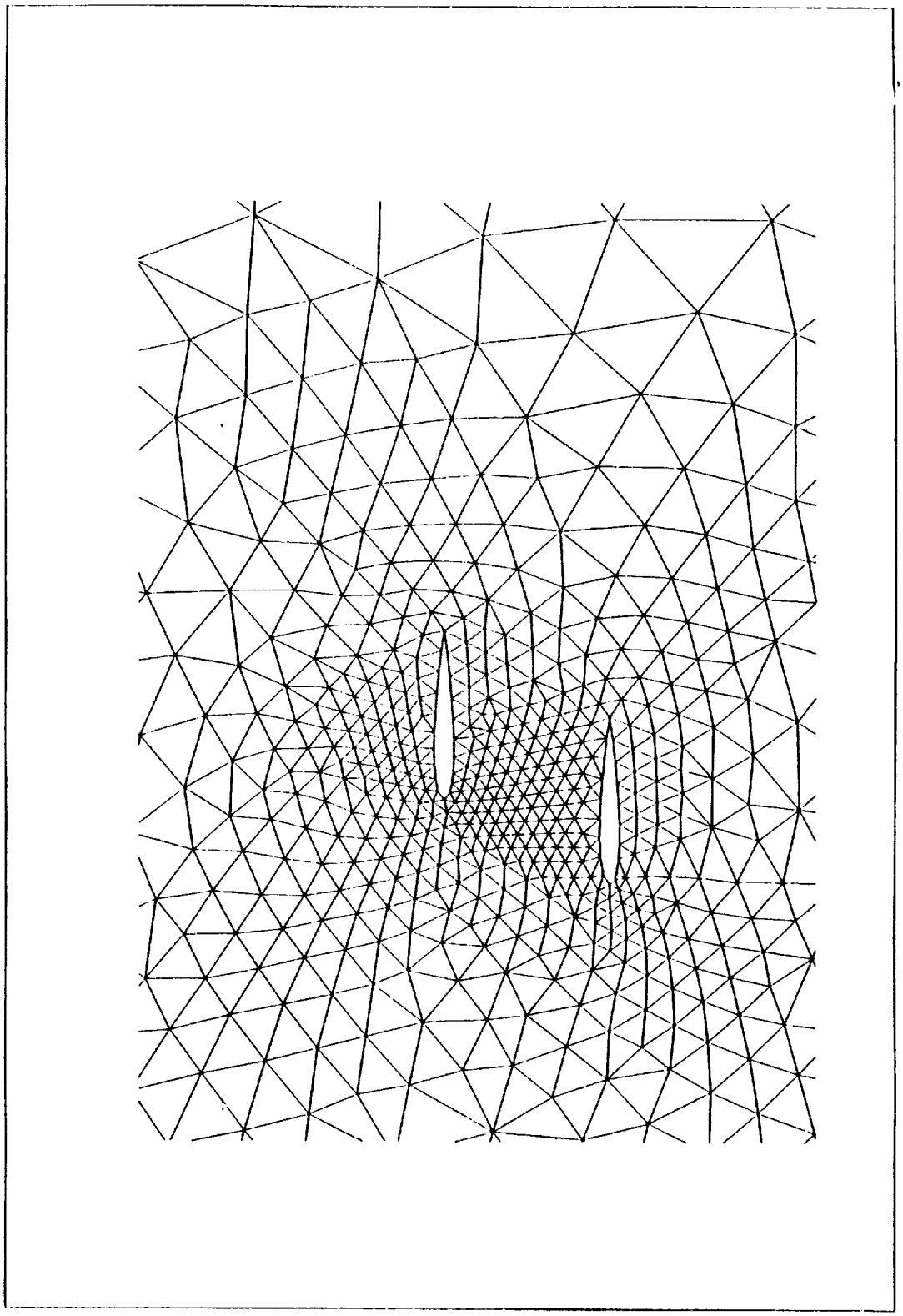

Fig. 4.35 Unstructured grid for a bi-plane.

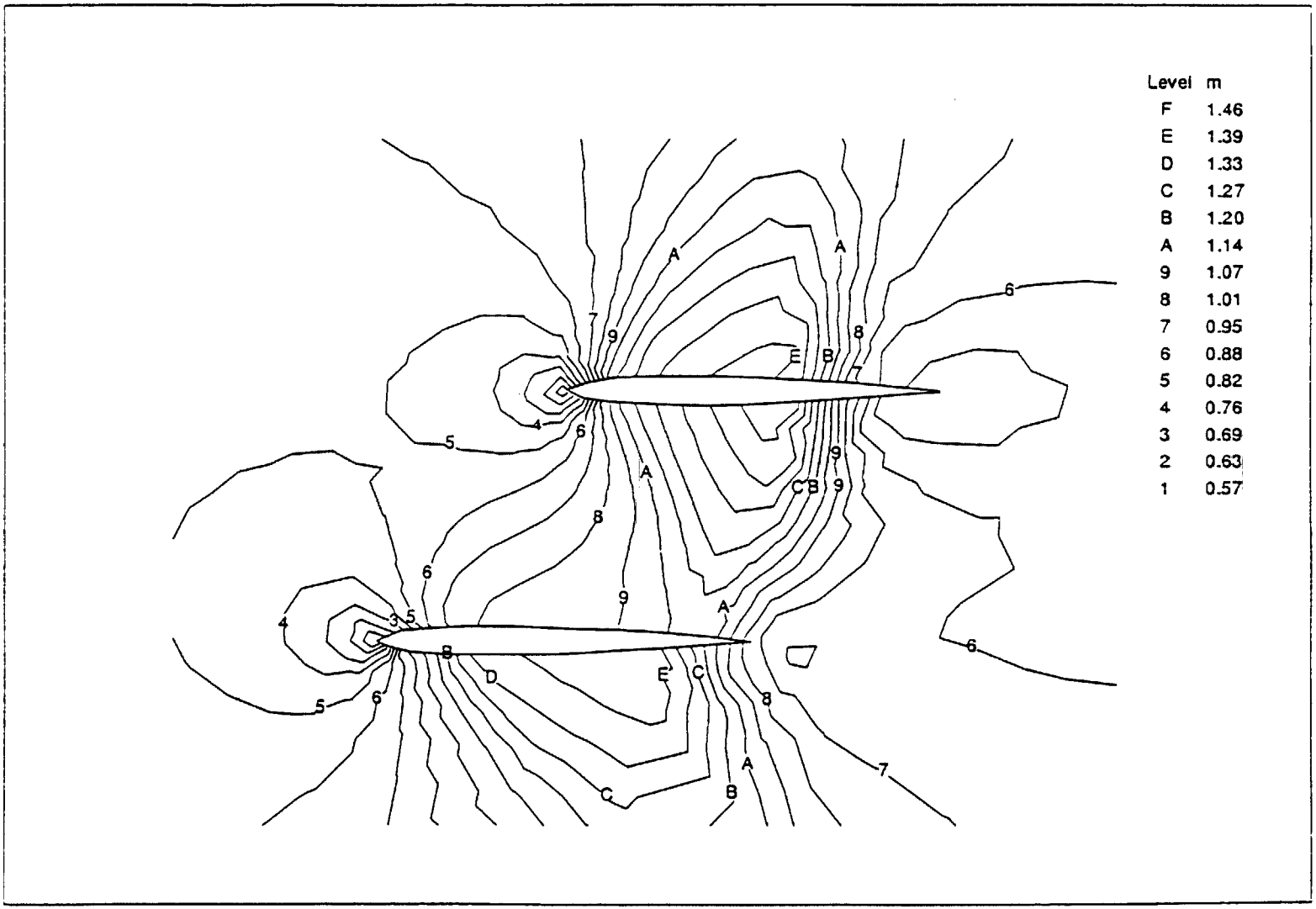

Fig. 4.36 Mach number contours for a bi-plane ($M_\infty = 0.84$, $\alpha = 0$).

and zero angle of attack. Overall, the Mach number contour plot in Fig. 4.36 is in good agreement with the results obtained by Hwang [7].

Case 5

In this case a four-element airfoil system is considered. The geometry represents a section of a wing in its landing configuration. Figure 4.37 shows the coarse mesh generated in 2-D with 5354 points, 10469 cells and 245 boundary points. Figure 4.38 shows the fine mesh consisting of 13898 points, 454 boundary points and 27348 cells.

The coarse mesh was taken for parametric study and run under the same conditions as that in Ref. [1] (ie. a Mach Number of 0.3 and 5 degrees angle of attack). Figure 4.39 shows the convergence history with first order differencing. The residuals dropped by about one and half orders of magnitude and then remained constant. Figure 4.40 shows the convergence history when the program was set for automatic selection of differencing. The program started with first order differencing and when the residuals dropped by one order of magnitude it switched over to second order. The jump in the curve shows the change in the order of differencing. The second order differencing however did not work as expected since a very coarse mesh was selected. The plots shown for the variation of different parameters are plotted for first order differencing.

Figure 4.41 shows the coefficient of pressure plotted over the top and bottom surfaces. The figure has the same trend as that shown in Ref. [1]. The variation in values are due to the fact that in Ref. [1] solution adaptive techniques are employed and hence a better grid point distribution is obtained.

Figures 4.42 and 4.43 show the Mach number and pressure contours. The plots are in good agreement with that shown in Ref. [8].

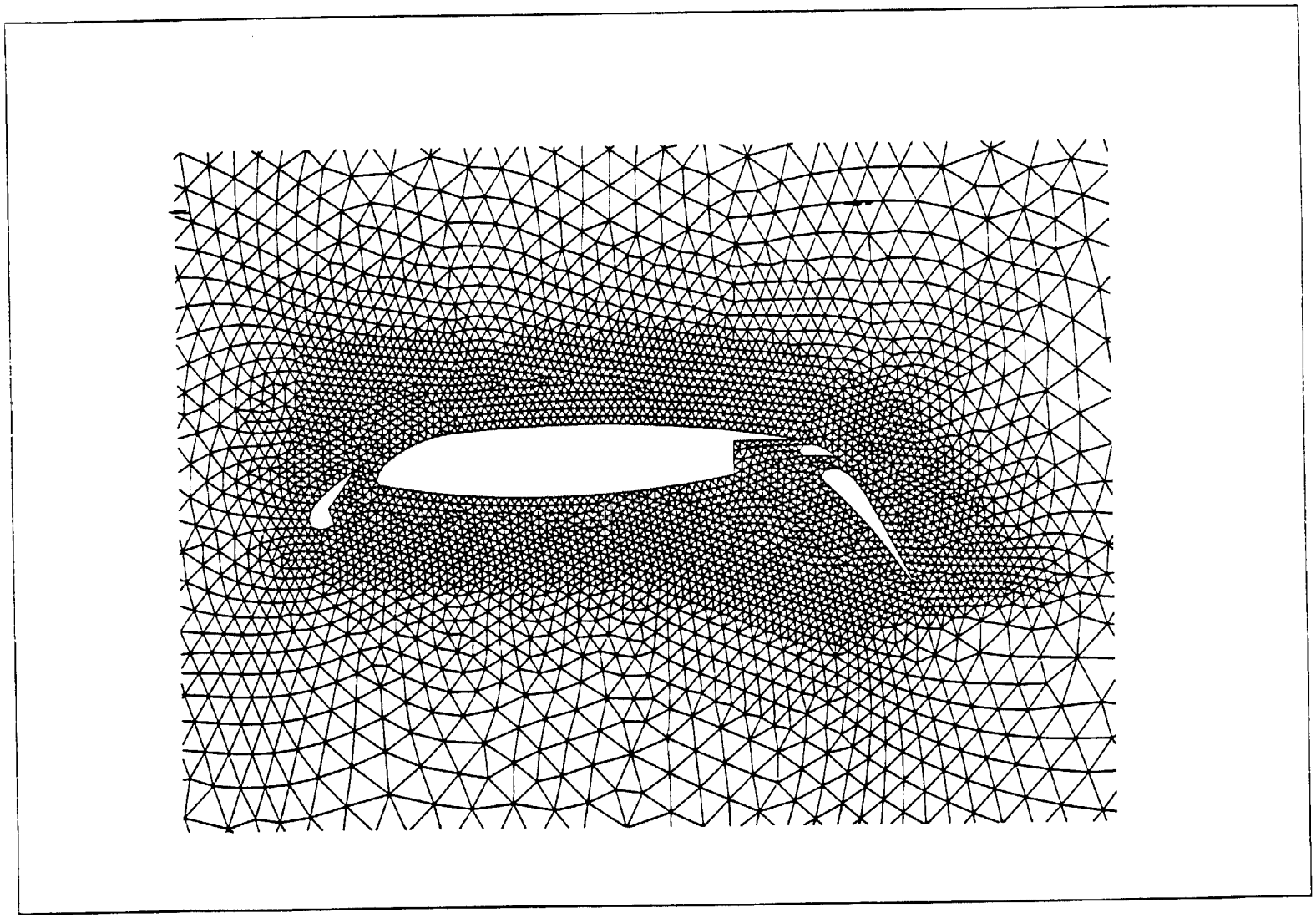

Fig. 4.37 Initial coarse mesh for a 4-element airfoil in its landing configuration.

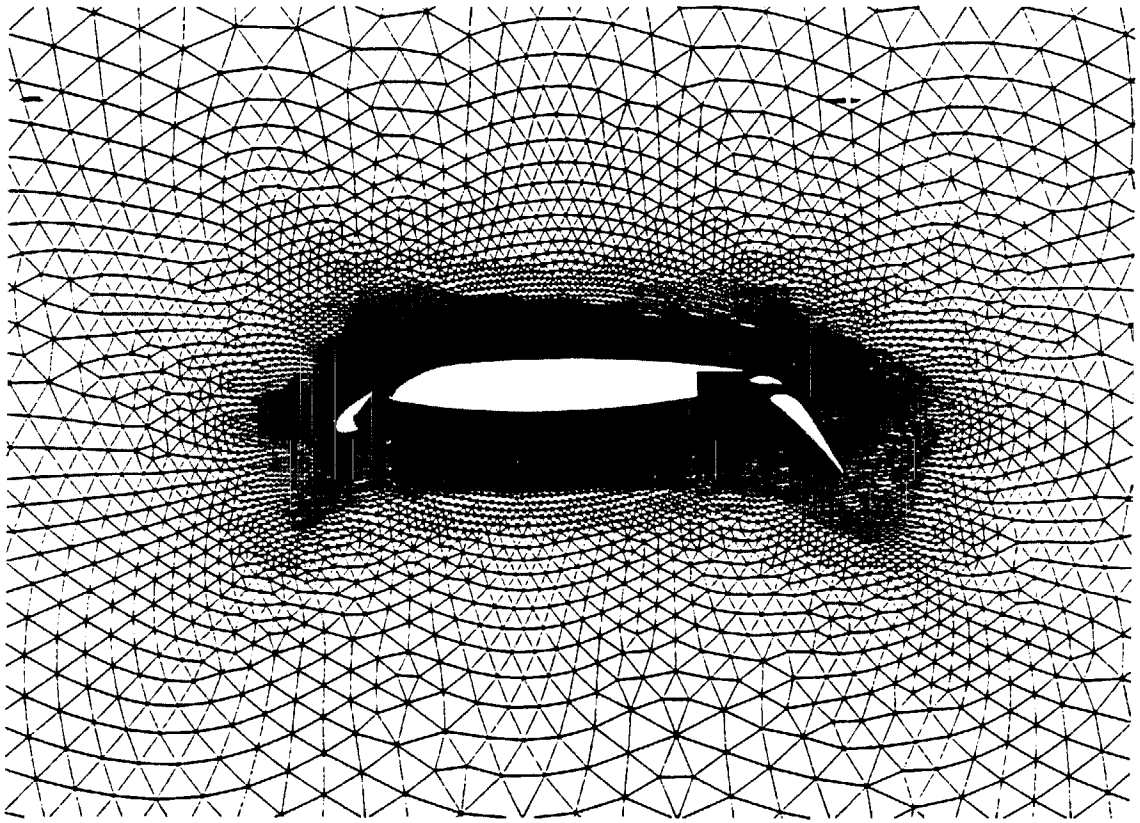

Fig. 4.38 Fine mesh for 4–element airfoil.

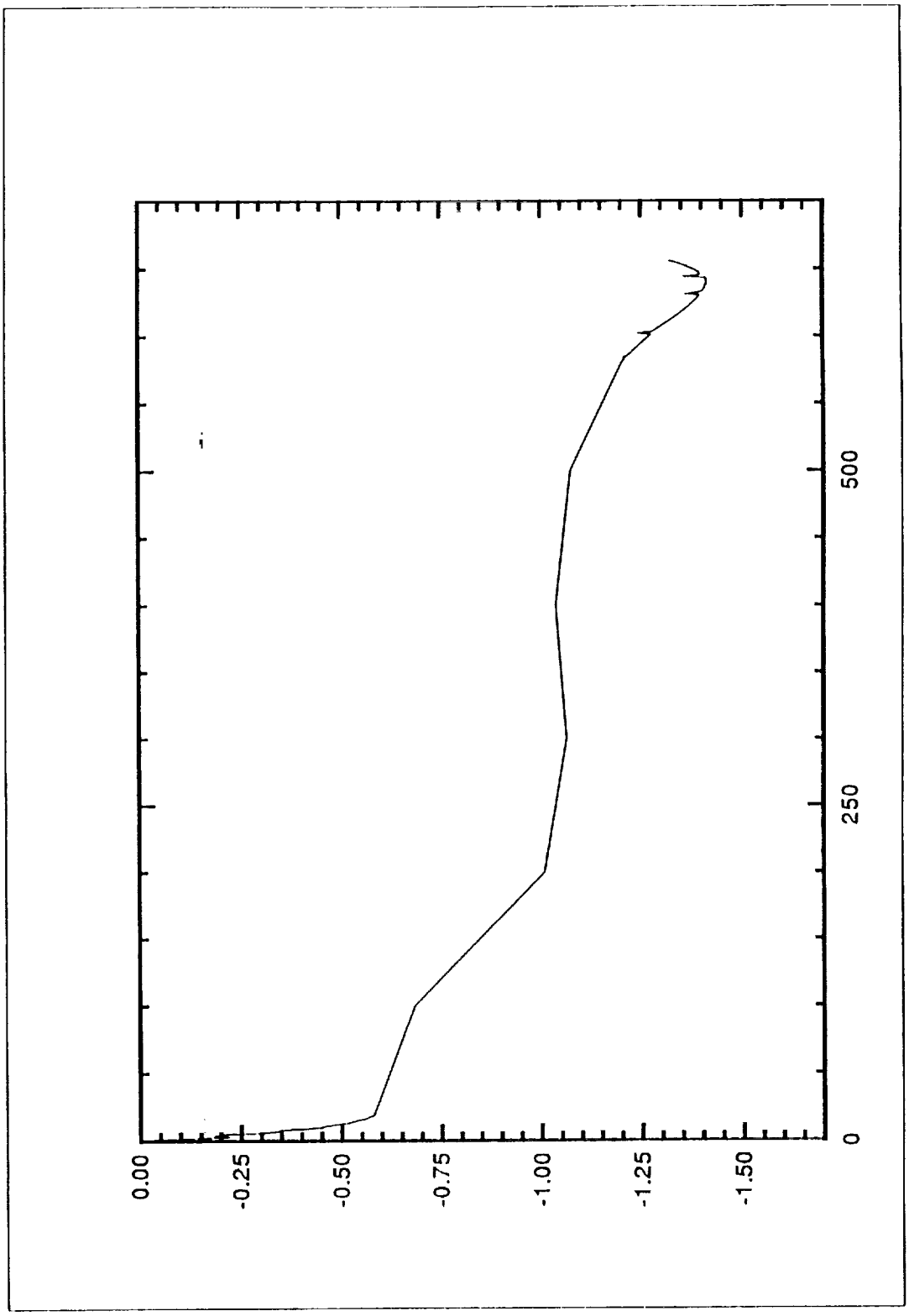

Fig. 4.39 Convergence history with first order differencing scheme.

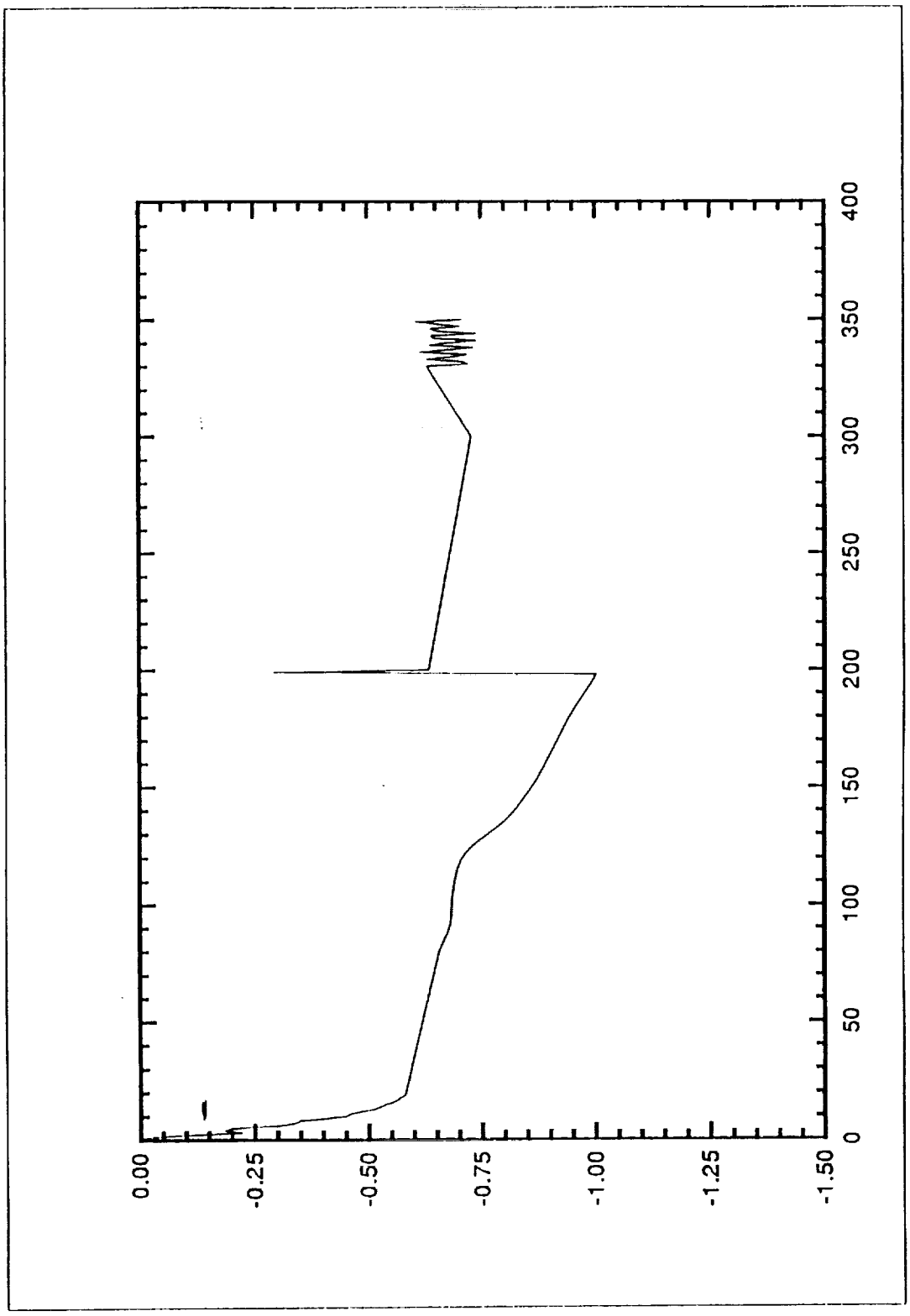

Fig. 4.40 Convergence history with automatic differencing scheme.

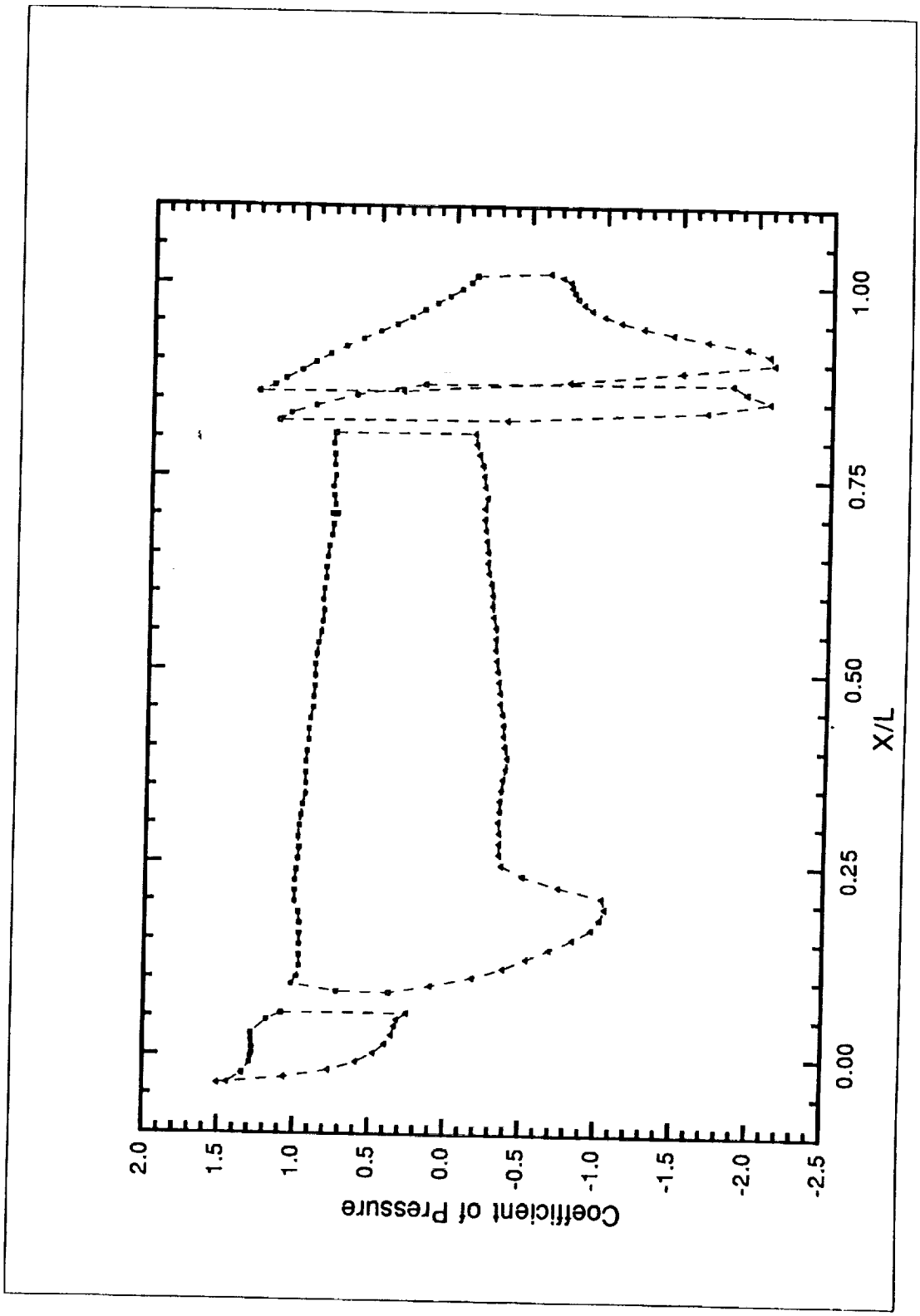

Fig. 4.4(Variation of coefficient of pressure over the upper and lower surface.

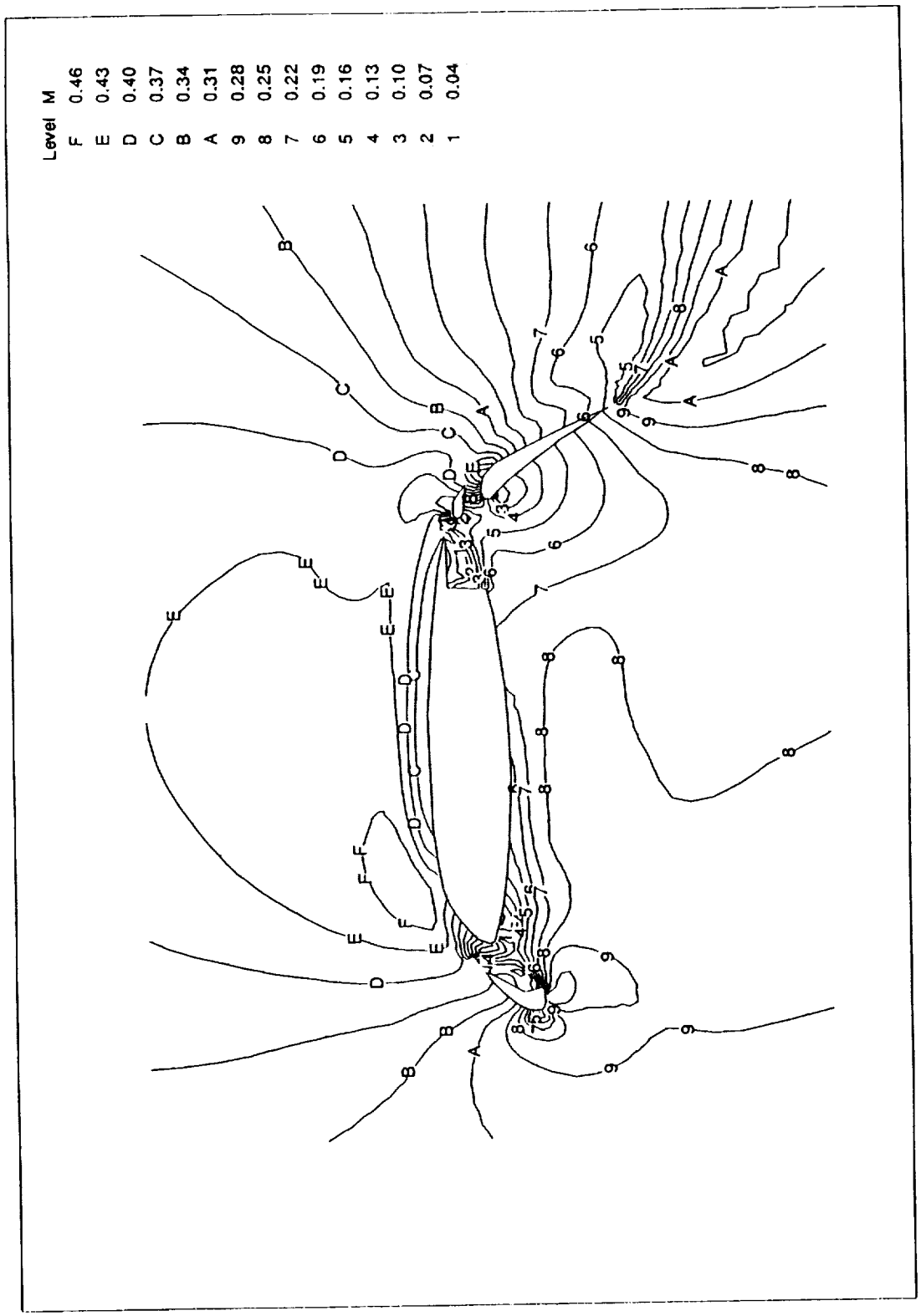

Fig. 4.42 Mach number contours for 4-element airfoil ($M_\infty = 0.3$, $\alpha = 5.0$).

Case 6

An ONERA M6 wing is used as a 3-D test case to generate unstructured grid. The wing has a leading edge sweep of 30 degrees, an aspect ratio of 3.8, taper ratio of 0.56, and symmetrical airfoil sections. The wing has a root chord of 0.67 and a semispan b of 1.0 with a rounded tip. The computational domain is bounded by a rectangular box with boundaries at $-6.5 \leq x \leq 11.0$, $0.0 \leq y \leq 2.5$ and $-6.5 \leq z \leq 6.5$. Transonic solutions are computed on the two grids shown in Figs. 4.44 and 4.45 at $M_\infty = 0.84$ and $\alpha = 3.06°$. The solutions were started with a free stream initial conditions with first order scheme and when the residuals dropped by one order of magnitude, at which the solver automatically switched over to higher order scheme. A comparison of wing surface pressure contours for the two mesh is shown in Figs. 4.46 and 4.47. The contours on both meshes show double shock wave on the upper surface. The contours on mesh2 show much sharper shock waves than the first one, demonstrating an effect of mesh density.

Coefficients of lift drag and pitching moment about the wing apex are given in Table 2. The table also shows the number of grid points and cells in each of the mesh used. The values are compared with that in Ref. [10].

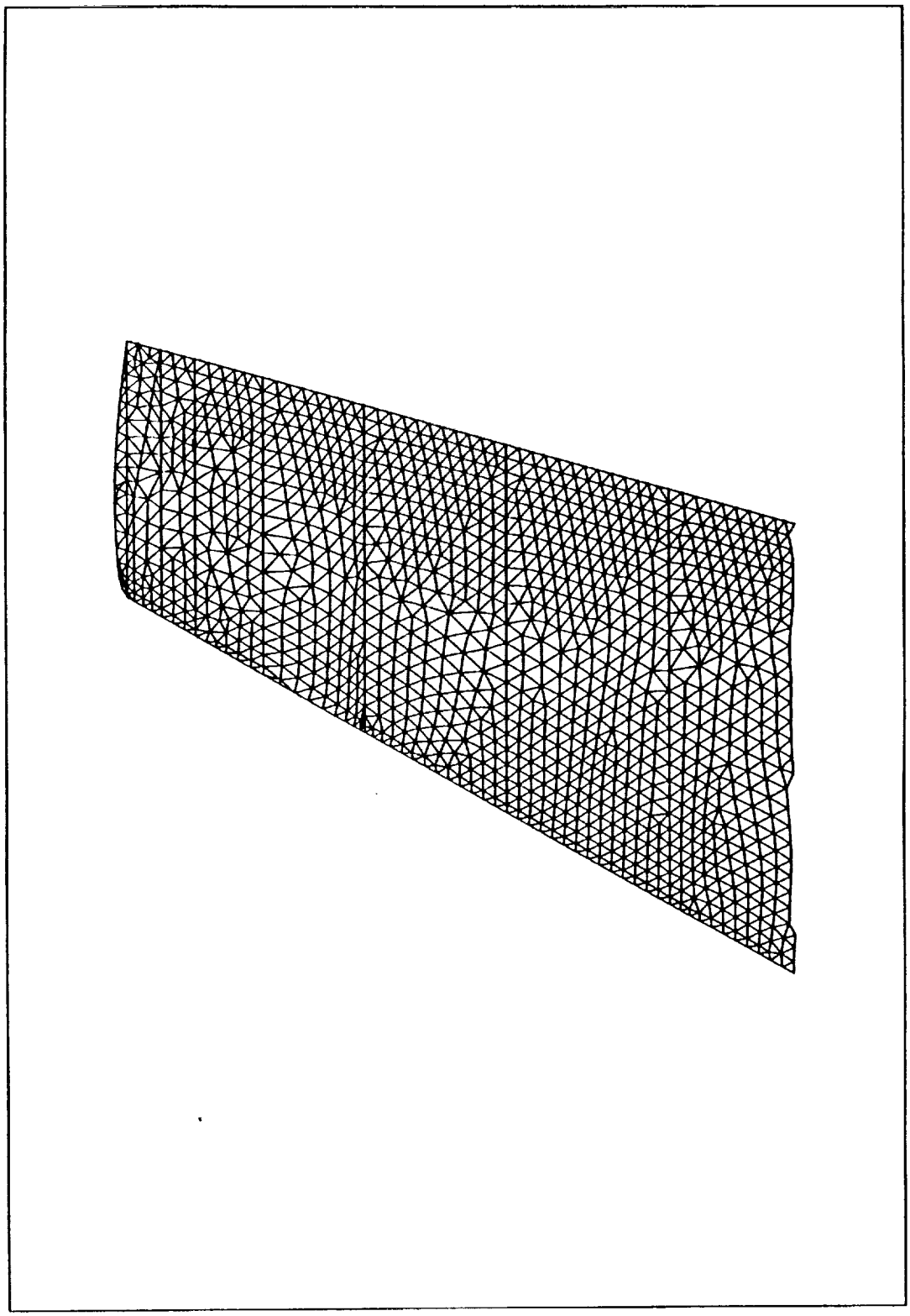

Fig. 4.44 Initial coarse mesh for ONERA M6 wing.

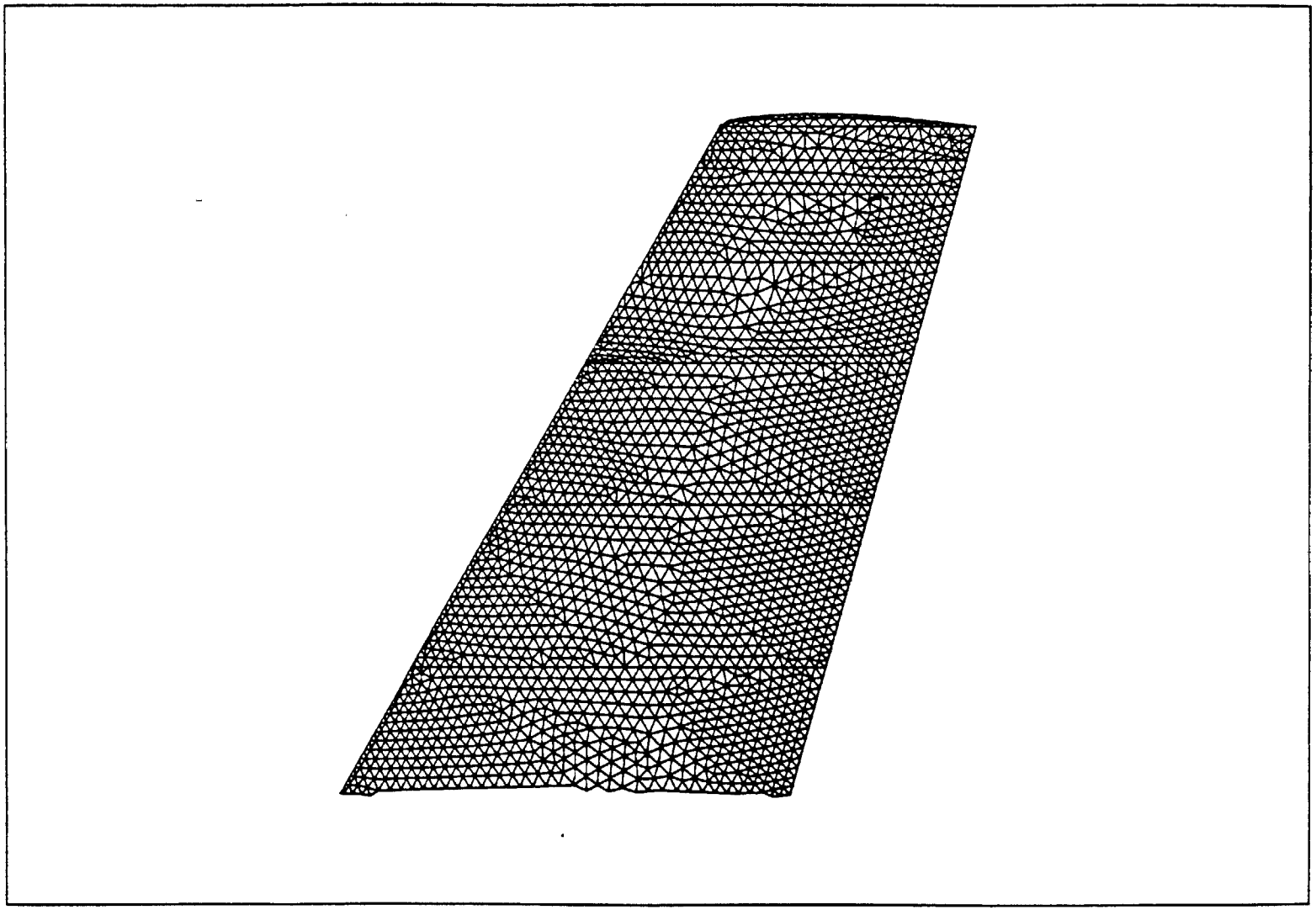

Fig. 4.45 Fine mesh for ONERA M6 wing.

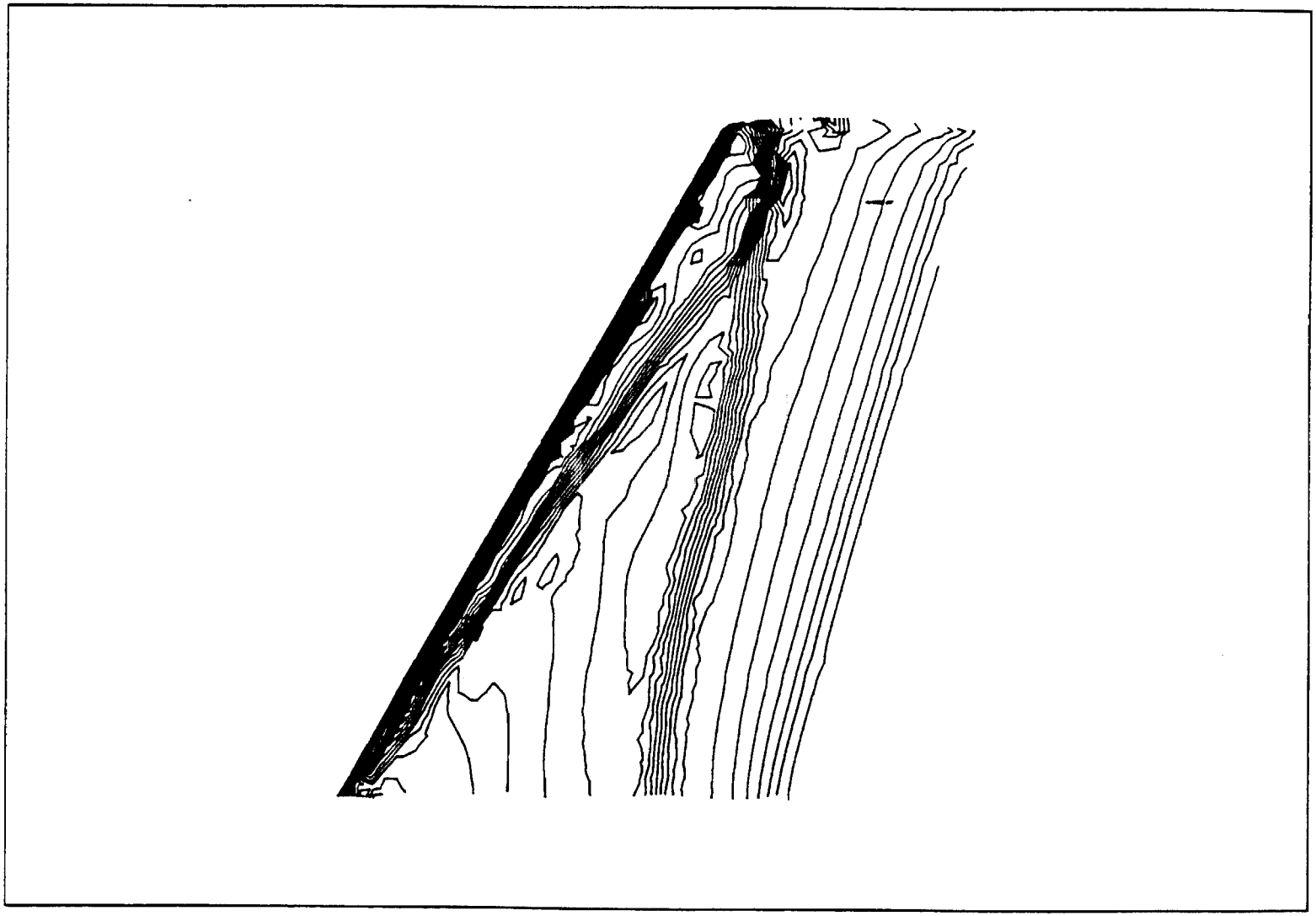

Fig. 4.46 Upper surface contour plot for the coarse mesh ($M_\infty = 0.84$, $\alpha = 3.06$, $\triangle p/p_\infty = 0.02$).

	Mesh 1	Mesh 2
Number of Cells	45,335 / 47,344*	94,257 / 98,317*
Number of Nodes	9,062 / 9,401*	18,357 / 19,048*
Number of Boundary Faces	2,829 / 2,932*	5,146 / 5,196*
Lift Coefficient	0.2879 / 0.2892*	0.2912 / 0.2893*
Drag Coefficient	0.0184 / 0.0195*	0.0154 / 0.0167*
Moment Coefficient	-0.1726 / -0.1715*	-0.1733 / -0.1702*

* Values taken from Ref.

Table 2. Comparison of ONERA M6 wing values with Ref. [10]

5. CONCLUDING REMARKS

In this study the superiority of unstructured grid over structured grid is demonstrated. Unstructured grids generated by VGRID3D software is compared with structured grids generated by GRIDGEN code. Specific problems considered are NACA 0012 airfoil, bi-plane consisting of two NACA 0012 airfoils, a four element airfoil in its landing configuration and an ONERA M6 wing. Inviscid time dependent solutions are computed for these geometries and compared with standard test results. A grid convergence study is conducted for NACA 0012 airfoil and compared with structured grid. The results obtained by NACA 0012 airfoil using unstructured grid showed an asymmetric distribution of flow field quantities and a fine distribution of grid was required to remove this asymmetry. On the other hand, the structured grid predicted a very symmetric distribution, but when the total number of points were compared the structured grid required more number of points.

For future studies its is recommended that unstructured grids be used with improved surface definition like (NURBS) around complex configurations. It is also advocated that refined model geometry be created before analyses are performed. Three-dimensional prismatic elements which are structured in the normal direction and unstructured in the axial direction will be a good test case for incorporating viscous terms.

REFERENCES

1. Mavriplis, D. J., "Accurate Multigrid Solution of the Euler Equations on Unstructured and Adaptive Meshes", AIAA Journal, Vol. 28, No. 2, February 1990, pp. 213-221.

2. Yerry, M. A. and Shepard, M. S., "Automatic Three-Dimensional Mesh Generation by the Modified-Octree Technique", International Journal of Numerical Methods in Engineering, Vol. 20, March 1984, pp. 1965-1990.

3. Löhner, R. and Parikh, P., "Generation of Three-Dimensional Unstructured Grids by the Advancing Front Method", International Journal Numerical Methods Fluids, Vol. 8, September 1988, pp. 1135-1149..

4. Steibnenner, J. P., Chawner, J. R. and Fouts, C. L., "The GRIDGEN3D Multiple Block Grid Generation System," General Dynamics Corporation, July 1990.

5. Frink, N. T., Parikh, P. and Pirzadeh, S., "A Fast Upwind Solver for the Euler Equations on Three-Dimensional Unstructured Meshes", AIAA Paper No. 91-0102, January 1991.

6. Rumsey, C. L., Taylor, S. L., Thomas, J. L. and Anderson, W. K., "Application of an Upwind Navier-Stokes Code to Two-Dimensional Transonic Airfoil Flow," AIAA Paper No. 87-0413, January 1987.

7. Harris, C. D., "Two Dimensional Aerodynamic Characteristics of the NACA 0012 Airfoil in the Langley 8-Foot Transonic Pressure Tunnel,"NASA TM-81927, April 1981.

8. Mavriplis, D. J., "Euler and Navier-Stokes Computations for Two-Dimensional Geometries Using Unstructured Meshes", NASA-CR-181977, January 1990.

9. Hwang, C. J. and Liu, J. L., "Locally Implicit Total-Variation-Diminishing Schemes on Unstructured Triangular Meshes", AIAA Journal, Vol. 29, No. 10, October 1991, pp. 1619–1626.

10. Woodard, P. R., Batina, J. T. and Yang, H. T. Y., "Quality Assessment of Two- and Three-Dimensional Unstructured Meshes and Validation of an Upwind Euler Flow Solver", AIAA Paper No. 92–0444, January 1992.

11. Thompson, J. F., Warsi, Z. U. A. and Mastin, C. W., Numerical Grid Generation: Foundations and Applications, North Holland, 1985.

12. Smith, R. E. and Eriksson, L. E., "Algebraic Grid Generation", Computational Methods Applications in Mechanical Engineering, Vol. 64, April 1987, pp. 285–300.

13. Smith, R. E. and Wiese, M. R., "Interactive Algebraic Grid Generation Technique", NASA Technical Paper 2533, March 1986.

14. Smith, R. E. (Ed.), Numerical Grid Generation Techniques, NASA Conference Publication 2166, NASA Langley Research Center, 1980.

15. Weatherill, N. P., "A Method for Generating Irregular Computational Grids in Multiply Connected Planer Domains", International Journal of Numerical Methods in Fluids, Vol. 8, August 1988, pp. 181–197